

A CORRELATION BETWEEN THE INTRINSIC BRIGHTNESS AND AVERAGE DECAY RATE OF GAMMA-RAY BURST X-RAY AFTERGLOW LIGHT CURVES

J. L. RACUSIN^{1,2}, S. R. OATES^{3,4}, M. DE PASQUALE⁴, AND D. KOCEVSKI¹

ACCEPTED FOR PUBLICATION IN APJ

ABSTRACT

We present a correlation between the average temporal decay ($\alpha_{X,avg,>200s}$) and early-time luminosity ($L_{X,200s}$) of X-ray afterglows of gamma-ray bursts as observed by *Swift*-XRT. Both quantities are measured relative to a rest frame time of 200 s after the γ -ray trigger. The luminosity average decay correlation does not depend on specific temporal behavior and contains one scale independent quantity minimizing the role of selection effects. This is a complementary correlation to that discovered by Oates et al. (2012) in the optical light curves observed by *Swift*-UVOT. The correlation indicates that on average, more luminous X-ray afterglows decay faster than less luminous ones, indicating some relative mechanism for energy dissipation. The X-ray and optical correlations are entirely consistent once corrections are applied and contamination is removed. We explore the possible biases introduced by different light curve morphologies and observational selection effects, and how either geometrical effects or intrinsic properties of the central engine and jet could explain the observed correlation.

Subject headings: γ -ray sources; γ -ray bursts; X-ray sources; X-ray bursts

1. INTRODUCTION

Observations and understanding of Gamma-ray Bursts (GRBs) has changed dramatically over the last decade with NASA's *Swift* Gamma-ray Burst Explorer mission (Gehrels et al. 2004). *Swift* has provided a vast database of both prompt emission observations with the Burst Alert Telescope (BAT; Barthelmy et al. 2005b), and early ($T_{start} < T_0 + 100$ s) afterglow observations with the X-ray Telescope (XRT; Burrows et al. 2005) and with the Ultraviolet Optical Telescope (UVOT; Roming et al. 2005). Correlations between observable parameters in GRBs are plentiful but at present, most are not well understood. The relationships between the physical and geometrical effects needs to be separated in order to determine the true nature of GRB progenitors and jet physics of the central engine.

Oates et al. (2012, 2015) presented a correlation between the early-time ($t_{rest,200s} = t_{obs}/(1+z) = 200$ s, hereafter abbreviated t_{200s}) luminosity ($L_{O,200s}$) of a GRB optical afterglow light curve and the average decay rate of that light curve ($\alpha_{O,avg,>200s}$) from t_{200s} onward, measured by fitting a power law, with a linear relationship $\alpha_{O,avg,>200s} = (-0.28 \pm 0.04) \log L_{O,200s} + (7.72 \pm 1.31)$, with a Spearman rank correlation coefficient (hereafter R_{sp}) of -0.58 and a null hypothesis of 1.90×10^{-5} . This qualitatively implies that initially brighter GRB afterglows decay faster and fainter afterglows decay slower. In this paper, we aim to search for this same correlation with X-ray afterglow observations. X-ray light curves have been shown to typically contain more complex structure than optical light curves (Panaitescu 2007; Liang et al. 2008; Evans et al. 2009), as the morphology

tends to be the convolution of the prompt emission internal dissipation mechanisms and the afterglow forward shocks. Therefore, the average decay rate depends on which light curve segments are included, which in turn depends on the assumptions on the physical origins of these segments.

Other trends and correlations have been demonstrated for X-ray afterglows including some evidence for clustering in luminosity with the brighter afterglows decaying faster than the fainter ones (Boër & Gendre 2000; Gendre & Boër 2005), though that clustering has disappeared with larger samples (Gendre et al. 2008; Bardho et al. 2015); a correlation between the luminosity and time of the end of the plateau (Dainotti et al. 2010, 2013; Sultana et al. 2013), and correlations with prompt emission parameters (Gehrels et al. 2008; Dainotti et al. 2011; D'Avanzo et al. 2012; Margutti et al. 2013).

The data reduction and analysis including sample selection and light curve fitting, will be discussed in §2, the results of the correlation tests in §3, observational biases, other X-ray afterglow correlations, and possible physical origin are discussed in §4, and conclusions in §5. Throughout this work, the convention $F(t) \sim t^{-\alpha} \nu^{-\beta}$ is used, where α is the temporal power-law index and β is the spectral energy index. Note that Oates et al. (2012, 2015) use the negative of this convention. All errors are 68% confidence unless stated otherwise, and we assume cosmological parameters of $H_0 = 70$ km s⁻¹ Mpc⁻¹, $\Omega_\Lambda = 0.7$ and $\Omega_m = 0.3$.

2. DATA REDUCTION AND ANALYSIS

2.1. Sample Selection

All *Swift*-BAT discovered GRBs, with X-ray afterglows detected by *Swift*-XRT and measured redshifts, discovered between December 2004 and March 2014 are included in the following analysis. Only those bursts with redshifts can be used, because the correlation parameters depend on intrinsic luminosity at the same relative redshift-scaled time. We include only those X-ray after-

¹ NASA's Goddard Space Flight Center, Code 661, Greenbelt, MD

² judith.racusin@nasa.gov

³ Instituto de Astrofísica de Andalucía (IAA-CSIC), Glorieta de la Astronomía s/n, E-18008, Granada, Spain

⁴ Mullard Space Science Laboratory, University College London, Holmbury St. Mary, Dorking, Surrey RH5 6NT

glows with at least 3 light curve bins ($\gtrsim 60$ counts), such that we have sufficient statistics to constrain the temporal and spectral fits, and T_{90} measurements are available in the BAT catalogs (Sakamoto et al. 2008, 2011; Lien et al. 2015). There are 280 GRBs in our sample that fit this criteria. As described in §3.2, we compare the correlation for both short and long duration GRBs, but primarily focus on long bursts, as short bursts to a large extent have different light curve morphology, environments, and energetics. The early average decay - luminosity correlation focuses on early-time flux estimates, therefore we also exclude any bursts for which observations started more than a factor of 2 after t_{200s} , such that extrapolation over long timescales could be inaccurate. The final sample includes 237 long GRBs (9 short), 47 of which also appear in the Oates et al. (2012, 2015) sample for the UVOT correlation (sample only extends through 2010). The redshift measurements come from a convolution of databases^{5,6} and the literature, and are listed in Table 2.

2.2. Light Curve Fitting

All light curves were retrieved from the University of Leicester *Swift* XRT Team GRB repository (Evans et al. 2007, 2009). The count rate light curves were converted to 0.3-10 keV flux using a single conversion factor from the automated repository spectral fits to the photon counting (PC) mode data. XRT switches to PC mode typically after the episodes of significant spectral evolution during flares and steep decay segments, yet while the afterglow is bright enough to accumulate sufficient statistics for a well-measured spectrum. However, all light curve fitting, as described in this section, was done in the count rate domain.

The flux light curves were converted to 1 keV flux density using the spectral index from the automated PC fits, and then to intrinsic luminosity, and k-corrected using the following formula:

$$L(t) = F_\nu(t) \times 4\pi D^2 (1+z)^{(\beta-1)}, \quad (1)$$

where $L(t)$ is the luminosity at any given time, $F_\nu(t)$ is the 1 keV flux density, D is the luminosity distance, and z is the redshift.

The BAT trigger time, T_0 , is generally used as the zero point of light curve analysis. However, T_0 for each GRB is a quantity determined by one of hundreds of onboard trigger criteria, and as such, is an empirical quantity, not a physical measure of the burst onset. While it typically does well as an indication of onset, occasionally emission is clearly visible prior to T_0 . The standard measurement of GRB duration - the time in which 90% of the fluence (time-integrated flux) is emitted (T_{90}) - is at least a characterization of the measured emission, though can be significantly flawed in cases with multiple emission episodes with quiescent emission in between, and varies with the relative level of signal and noise. In the BAT automated and catalog temporal analyses (Sakamoto et al. 2008, 2011; Lien et al. 2015), T_{90} is measured between T_{05} and T_{95} , which represents the 5% and 95% limits on the BAT GRB emission. In this paper, we use the time

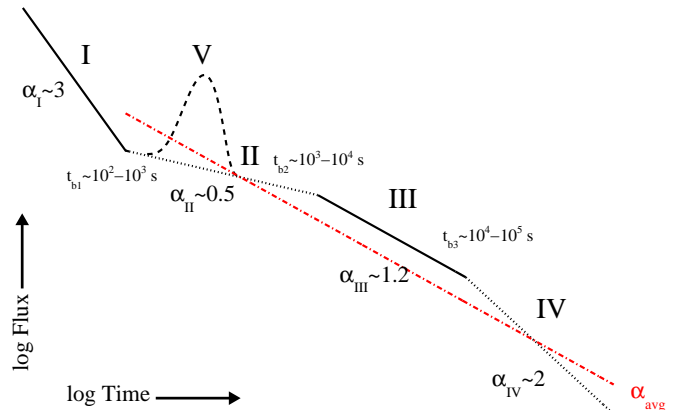


Figure 1. Morphology of canonical GRB X-ray afterglow (Zhang et al. 2006; Nousek et al. 2006) and comparison to average afterglow. Segments are generally attributed to: I) steep decay due to curvature effect of delayed prompt emission; II) plateau due to some form of continued energy injection; III) normal forward shock decay of the afterglow; IV) the post-jet break decay; and V) flares that are seen in $\sim 1/2$ of all GRBs. The measurements of the average decay rate are described in §2.2. Slopes and break times have broad distributions (see Racusin et al. 2009; Evans et al. 2009.)

T_{05} instead of T_0 as the light curve zero point. In 64% of GRBs in our sample, T_0 and T_{05} differ by less than 5 seconds, and less than one minute in 96% of the sample, with extreme cases (likely due to *Swift* slewing at the time of emission onset or another instrumental delay) deviating by as much as 200-300 seconds. The average decay rate is typically affected by the shift of T_0 with a change in slope < 0.1 . All BAT parameters were taken from the BAT catalogs (Sakamoto et al. 2008, 2011; Lien et al. 2015).

GRB X-ray afterglow light curves demonstrate complex and highly varied structure, and typically contain up to 5 components (Figure 1): I) a steep decay lasting tens to hundreds of seconds likely related to the tail of the prompt emission generally attributed to the curvature effect; II) a plateau lasting hundreds to thousands of seconds which is generally attributed to some sort of energy injection boosting the forward shock emission; III) the normal forward shock power-law decay; IV) a post-jet break decay; and V) in some cases flares which can occur during any phase and be either single emission episodes or in multiple (Zhang et al. 2006; Nousek et al. 2006), and an occasional flat segment prior to the steep decay labeled as 0, which is part of the prompt emission. While the majority of bursts can be characterized as displaying some of the canonical components, very few rarely display them all, and significant deviations such as single power-law behavior is common (Racusin et al. 2009; Evans et al. 2009).

In our previous works (Racusin et al. 2009, 2011), we have characterized the best-fit power-laws to the full sample of X-ray afterglows. We have since added Gaussians to characterize X-ray flares, rather than removing the interval by eye from the fitted data. Our process still requires user input, and is only semi-automated. The power law fits with up to 5 breaks are used as a way to differentiate the internal (steep decay/flares) versus external (plateaus, normal, post-jet break) shock portions

⁵ <http://www.mpe.mpg.de/~jcgrbgen.html>

⁶ <http://www.astro.caltech.edu/grbox/grbox.php>

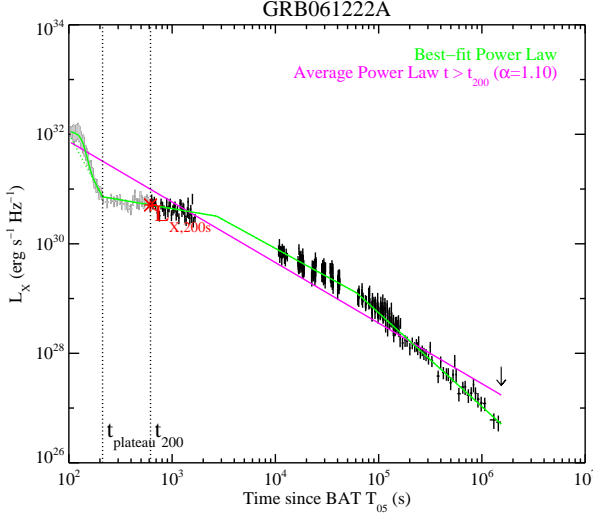


Figure 2. Light curve and fits to GRB 061222A, an example X-ray afterglow that displays the canonical best-fit power law (PL) segments (green), and a single average power law fit (magenta) demonstrating our measure of average decay rate ($\alpha_{X,avg,>200s}$). The luminosity $L_{X,200s}$ is extracted from the best fit (power-law) models at t_{200s} . The points excluded from the average power-law models are in gray.

of the light curves. These fits to all segments I-V will be hereafter referred to as “best-fit (power-law) models” (i.e. Figure 1). We measure an early characteristic luminosity, $L_{X,200s}$ at 1 keV, by extrapolating or interpolating the luminosity at t_{200} from the best fit (power-law) models depending on when the observations began. The temporal decay index from the best fit (power-law) models at t_{200s} is referred to as $\alpha_{X,fit,200s}$.

We attempt to characterize average behavior (hereafter referred to as “average power-law models”), not focusing on the details that affect the individual slopes such as the density profile of the circumburst environment, location and evolution of the cooling break in the Synchrotron spectrum (Sari et al. 1998), and the microphysical parameters (electric and magnetic field contribution, density of environment, radiative efficiency). Therefore, the simplest way to measure the average decay rate ($\alpha_{X,avg,>200s}$) is to fit a simple power-law to the complex light curve of the X-ray afterglow (Figure 2), after some specific rest frame time, for which we use $t_{200s} = 200 \times (1 + z)$. While this is most likely a very poor fit statistically, it is a adequate characterization of the average behavior.

Complications affect X-ray light curves more so than their optical correlaries including the tail of the prompt emission, and early- and late-time flares. Therefore in §3 and Figure 4, we will demonstrate the luminosity-average decay correlation without performing any corrections to the light curves. In the following, we demonstrate step-by-step how our correlation is improved if we exclude these additional components from the measures of $L_{X,200s}$ and $\alpha_{X,avg,>200s}$.

The average power-law model is dominated by the portion of the light curve with the best statistics - the early bright part (often Segment I), which is also most likely to be related to the prompt emission, not the afterglow (Zhang et al. 2007). For those cases where the average

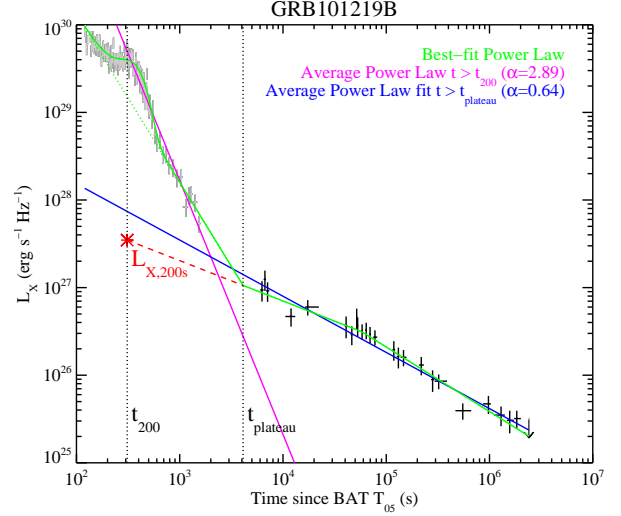


Figure 3. Fits to the X-ray light curve of GRB 101219B, for which the uncorrected average decay (magenta) is contaminated by the steep decay segment (Segment I). As described in the text, we wish to characterize only the external shock afterglow, and therefore fit the average decay after the transition from steep to shallow decay ($t > t_{plateau}$, Segments II-IV, blue), and extrapolate the best fit (power-law) models back to t_{200s} to measure $L_{X,200s}$ (red). The initial average power law fit for $t > t_{200s}$ (magenta) is much steeper than the corrected average power law fit to $t > t_{plateau}$ (blue). The points excluded from the average power-law models are in gray.

decay is dominated by the steep decay (i.e. it ends after t_{200s}), we correct their average decay fits by including only the data after the end of the steep decay (Segments II-IV identified through the best fit (power-law) models, see §3.1 for details). In these cases $L_{X,200s}$ will also be dominated by the prompt emission. To obtain a luminosity representative of the afterglow at that time we extrapolate Segment II of the best fit (power-law) models back to t_{200s} . Figure 3 demonstrates an example case that we correct for steep decay contamination in the average decay and luminosity.

Cases where there are flares after t_{200s} (or the start of the plateau, if later), may also be significantly biased by the bright light curve points during flares that dominate the emission. We test the impact of flares on the average decay-luminosity correlation in §3.3, and alleviate this issue by excluding all the of the light curve points that contain flaring intervals when fitting the average power-law model.

2.3. Correlation Analysis

In order to determine the strength and significance of each correlation, we perform a linear regression analysis using the IDL astrolib⁷ routine *fitxy*. The advantage of this tool is that it utilizes errors on both parameters, and is reverseable if one switches the axes of the input parameters. Therefore, it does not require a dependent variable. From this regression analysis, we measure the slope of the relation and a constant offset (Table 1). Although *fitxy* accounts for the errors on both parameters, it does not address the intrinsic dispersion. Consequently, we find a reduced $\chi^2 \gg 1$, and therefore the covariance errors are not reliable. To overcome this limi-

⁷ <http://idlastro.gsfc.nasa.gov/>

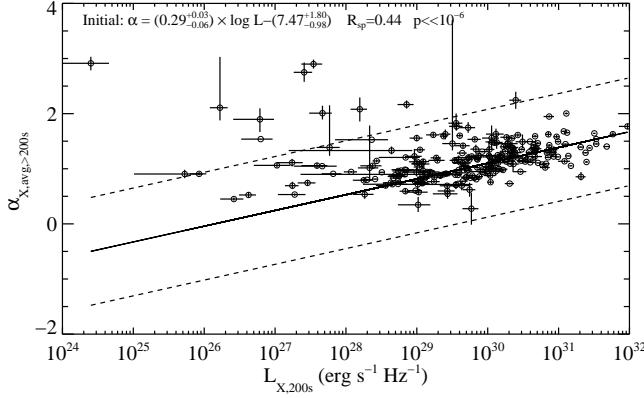


Figure 4. Average decay - luminosity correlation using the full sample with no optimizations, corrections or filtering. There is significant scatter at low luminosities which will be addressed in §3. The best fit regression parameters and their 1σ errors, and the Spearman rank coefficient and associated probability are listed on the plot and in Table 1. The solid line indicates the best fit regression, and dashed lines indicates the 2σ deviation.

tation, we determine the errors via a Monte Carlo Bootstrap calculation. For 10^4 trials, we randomly selected a subset of our data sample that is the same size as our data sample, allowing for possible duplicated values (i.e. sampling with replacement), and redo the linear regression. The resulting distributions of slope and constant offset for each trial, allow us to extract the 1σ errors on each parameter.

We determine the strength of the correlation by measuring a Spearman rank coefficient (R_{sp}), and its corresponding null hypothesis probability (p) using the IDL tool *r.correlate*. We also test the dependence on the correlation between $L_{X,200s}$ and $\alpha_{X,avg,>200s}$ with redshift, a parameter with some dependence in both quantities. To do this, we conduct a partial Spearman rank correlation analysis. The correlation remains significant when accounting for redshift (Table 1), demonstrating that we are not simply correlating redshift with itself.

3. RESULTS

The following section describes the resulting luminosity - average decay correlation, and how we reduce the scatter, optimize the correlation, and investigate its origin. The correlation parameters for each iteration and subset are summarized in Table 1.

Similar to the correlation in Oates et al. (2012), we see evidence for a correlation (Figure 4) in our full sample, even without correcting for the steep decay contamination. Significant scatter is present in the relation, due to both the steep decay contamination discussed in §3.1, and fundamental differences in sub-samples (e.g. long/short duration, §3.2). The next section describes optimizations and tests for light curve morphological features that may influence the correlation and apparent scatter.

The presence of features in the afterglow light curves (plateaus, flares, etc.) could potentially influence or even be the root cause of the correlations. We test these effects, and other observational biases by splitting the sample and reproducing the same analyses in the following. Through these efforts we are able to reduce some of the sources of the scatter in the relation.

3.1. Steep Decay Contamination

As demonstrated in Figure 3, GRBs for which the steep decay continues past t_{200s} , have average light curve fits contaminated by that steep decay which is a distinct component from the afterglow in both temporal and spectral morphology. This affects both of our measurements of $\alpha_{X,avg,>200s}$ and $L_{X,200s}$. Of the 246 GRBs in our sample, 23 suffer from this contamination. In those cases, we fit the average light curve over the interval from the start of the plateau to the end of the light curve. A comparison between those bursts that do and do not require the steep decay correction show significant differences in the average decay-luminosity correlation using the uncorrected decay rates (Figure 5). All correlations presented in the rest of this paper apply the steep decay contamination correction to those 23 GRBs.

Sample	Parameters		Spearman Rank	Null Hypothesis	Partial Spearman Rank	Null Hypothesis	Best fit linear regression		Number in Sample
	x-axis	y-axis					Slope	Constant	
Initial	$\log L_{X,200s}$	$\alpha_{X,avg,>200s}$	0.44	$\ll 10^{-6}$	0.49	$\ll 10^{-6}$	$0.29^{+0.03}_{-0.06}$	$-7.47^{+1.80}_{-0.98}$	246
Steep Decay Contam	$\log L_{X,200s}$	$\alpha_{X,avg,>200s}$	-0.44	0.04	-0.10	> 0.10	$-0.83^{+0.48}_{-0.34}$	$25.72^{+9.69}_{-14.49}$	23
Not Contam	$\log L_{X,200s}$	$\alpha_{X,avg,>200s}$	0.56	$\ll 10^{-6}$	0.57	$\ll 10^{-6}$	$0.29^{+0.04}_{-0.30}$	$-7.52^{+8.97}_{-1.13}$	223
Short	$\log L_{X,200s}$	$\alpha_{X,avg,>200s}$	-0.07	> 0.10	0.11	> 0.10	$0.16^{+0.10}_{-0.39}$	$-3.40^{+11.16}_{-2.77}$	9
Long	$\log L_{X,200s}$	$\alpha_{X,avg,>200s}$	0.59	$\ll 10^{-6}$	0.59	$\ll 10^{-6}$	$0.27^{+0.04}_{-0.04}$	$-6.99^{+1.23}_{-1.10}$	237
Flares	$\log L_{X,200s}$	$\alpha_{X,avg,>200s}$	0.58	$\ll 10^{-6}$	0.56	$\ll 10^{-6}$	$0.30^{+0.07}_{-0.06}$	$-7.91^{+1.84}_{-2.17}$	134
No Flares	$\log L_{X,200s}$	$\alpha_{X,avg,>200s}$	0.59	$\ll 10^{-6}$	0.64	$\ll 10^{-6}$	$0.28^{+0.03}_{-0.04}$	$-7.27^{+1.28}_{-1.01}$	103
Plateau	$\log L_{X,200s}$	$\alpha_{X,avg,>200s}$	0.58	$\ll 10^{-6}$	0.55	$\ll 10^{-6}$	$0.26^{+0.05}_{-0.06}$	$-6.81^{+1.84}_{-1.43}$	156
No Plateau	$\log L_{X,200s}$	$\alpha_{X,avg,>200s}$	0.57	$\ll 10^{-6}$	0.61	$\ll 10^{-6}$	$0.26^{+0.06}_{-0.05}$	$-6.82^{+1.60}_{-1.83}$	81
Final	$\log L_{X,200s}$	$\alpha_{X,avg,>200s}$	0.59	$\ll 10^{-6}$	0.59	$\ll 10^{-6}$	$0.27^{+0.04}_{-0.04}$	$-6.99^{+1.23}_{-1.11}$	237
0	$\log L_{X,200s}$	$\alpha_{X,fit,200s}$	0.10	> 0.10	-0.58	> 0.10	$0.19^{+0.42}_{-0.16}$	$-5.10^{+5.12}_{-12.74}$	5
I	$\log L_{X,200s}$	$\alpha_{X,fit,200s}$	-0.24	0.05	-0.08	> 0.10	$-1.96^{+0.54}_{-0.55}$	$61.08^{+16.36}_{-16.22}$	70
II	$\log L_{X,200s}$	$\alpha_{X,fit,200s}$	0.16	0.09	0.15	> 0.10	$0.46^{+0.06}_{-0.25}$	$-13.19^{+7.57}_{-1.96}$	113
III	$\log L_{X,200s}$	$\alpha_{X,fit,200s}$	-0.06	> 0.10	-0.07	> 0.10	$-0.07^{+0.05}_{-0.03}$	$3.34^{+1.06}_{-1.53}$	36
IV	$\log L_{X,200s}$	$\alpha_{X,fit,200s}$	-0.20	> 0.10	-0.95	0.05	$-0.97^{+1.23}_{-3.06}$	$31.92^{+92.92}_{-38.56}$	4
SPL	$\log L_{X,200s}$	$\alpha_{X,fit,200s}$	0.28	> 0.10	0.30	> 0.10	$0.59^{+0.49}_{-1.14}$	$-16.63^{+34.45}_{-14.57}$	9
Only II	$\log L_{X,200s}$	$\alpha_{X,fit,II}$	0.23	1×10^{-3}	0.28	9×10^{-5}	$0.37^{+0.05}_{-0.21}$	$-10.26^{+6.28}_{-1.63}$	194

Only III	$\log L_{X,200s}$	$\alpha_{X,fit,III}$	0.04	> 0.10	0.03	> 0.10	$0.04^{+0.07}_{-0.07}$	$-0.06^{+2.22}_{-2.10}$	156
2004-2006	$\log L_{X,200s}$	$\alpha_{X,avg,>200s}$	0.50	2×10^{-5}	0.50	1×10^{-5}	$0.23^{+0.12}_{-0.08}$	$-5.80^{+2.29}_{-3.50}$	67
2007-2008	$\log L_{X,200s}$	$\alpha_{X,avg,>200s}$	0.73	$\ll 10^{-6}$	0.72	$\ll 10^{-6}$	$0.29^{+0.02}_{-0.06}$	$-7.55^{+1.78}_{-0.70}$	60
2009-2011	$\log L_{X,200s}$	$\alpha_{X,avg,>200s}$	0.54	4×10^{-6}	0.53	7×10^{-6}	$0.28^{+0.04}_{-0.03}$	$-7.17^{+1.03}_{-1.32}$	64
2012-2014	$\log L_{X,200s}$	$\alpha_{X,avg,>200s}$	0.61	6×10^{-6}	0.61	7×10^{-6}	$0.19^{+0.06}_{-0.06}$	$-4.62^{+1.66}_{-1.64}$	46
All	$\log L_{X,1day}$	$\alpha_{X,avg,>t_{plat}}$	-0.28	3×10^{-4}	-0.28	3×10^{-4}	$-0.15^{+0.07}_{-0.07}$	$5.53^{+2.04}_{-2.01}$	163

Table 1 Regression analysis results and correlation statistics for each subsample and correlation. The partial Spearman rank coefficient tests the dependence on GRB redshift. The significance columns apply to the regular or partial Spearman rank coefficient to the left of that column. Note that the subscripts “avg” and “fit” refer to the slope of the average temporal power law decay and the individual segment slopes of the best fit (power-law) models, respectively.

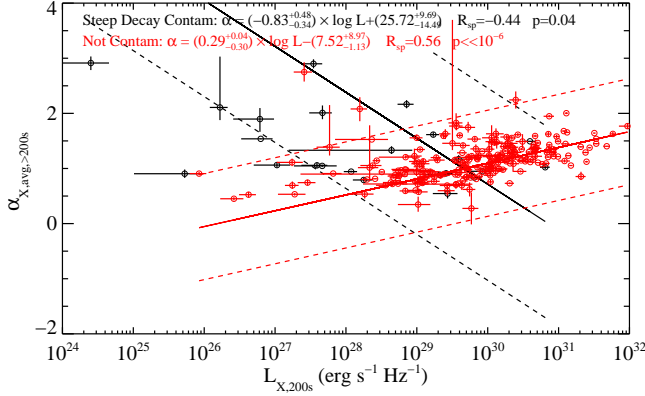


Figure 5. Average decay - luminosity correlation using the full sample with no optimizations, corrections or filtering. The sample is split between those that require a steep decay contamination correction (but have not yet received it), and those that do not require it. The sample that does not require the correction shows a significant correlation, while the sample that does require the correction shows no evidence for a significant correlation. The solid line indicates the best fit regression, and the dashed lines indicates the 2σ deviation.

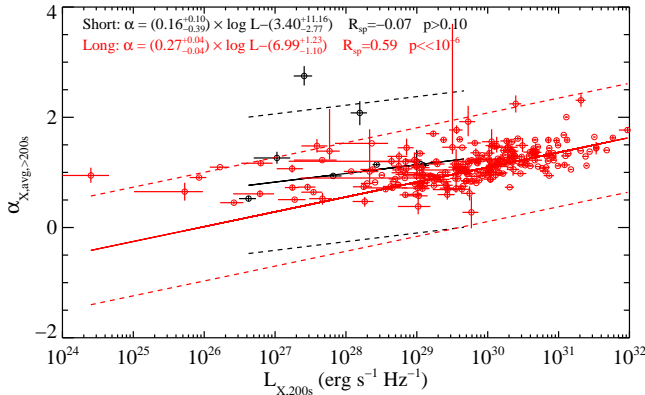


Figure 6. Average decay - luminosity correlation using the sample including steep decay corrections, and split by short ($T_{90} < 2s$) and long ($T_{90} > 2s$) prompt emission durations. The sample of short GRBs is small and does not show any evidence of a significant correlation. Short GRBs are removed for subsequent analyses. The solid line indicates the best fit regression, and the dashed lines indicates the 2σ deviation.

3.2. Short versus Long Duration GRBs

Short duration GRBs display both similarities and differences to long GRBs (Barthelmy et al. 2005a; Berger

2014), including: prompt emission spectral lags (Norris & Bonnell 2006; Norris et al. 2011), redshift distributions (Guetta & Piran 2006), prompt emission energetics (Amati et al. 2002; Ghirlanda et al. 2009), prompt emission light curves (Nakar & Piran 2002), prompt emission spectral properties (Goldstein et al. 2012), environments and host galaxies (Berger et al. 2007b; Troja et al. 2008; Fong et al. 2013), and afterglow properties (Kann et al. 2011; Racusin et al. 2009; Nysewander et al. 2009). While approximately half of all short GRB X-ray afterglows show long-lasting emission, the other half fade below the level of detectability within the first few thousand seconds, with on average steeper slopes than long GRBs, likely reflecting the lower density circumstellar environments). The so-called “naked GRBs” (Page et al. 2006; Perley et al. 2009a; Hascoët et al. 2011) may occur in such low density environments, in which they do not display forward shock emission, or the light curve decays below the detectability threshold during the steep decay phase.

We test for differences in the average decay-luminosity correlation between short and long duration GRBs (Figure 6), finding that long duration bursts are significantly correlated ($R_{sp} = 0.59$, $p = 1.01 \times 10^{-23}$) in the average decay-luminosity domain, and short bursts demonstrate no significant correlation ($R_{sp} = -0.07$, $p = 0.86$) and in fact include two of the points with the most deviant scatter. This suggests that the correlation is related to some difference between short and long GRBs in their the afterglow properties, be it environment or jet dynamics. For all further tests of the X-ray average decay-luminosity correlation, we exclude short GRBs.

3.3. X-ray Flares

X-ray flares have been extensively studied using early afterglow observations from XRT, and have been shown to have an internal rather than external shock origin (Falcone et al. 2007; Chincarini et al. 2007, 2010; Kocevski et al. 2007; Margutti et al. 2010). X-ray flares can occur at a variety of timescales and either as single or multiple pulses. As a potential source of contamination for the average decay-luminosity correlation, we separate those afterglows with X-ray flares (without removing flaring intervals) and those without flares (Figure 7), and find that the two samples show very similar correlation strengths and slopes, but with slightly more scatter in the sample with flares. Once we removed the intervals from the light curves with flares, defined as light curve bins where there is a $> 5\%$ deviation between fits with flares and that of the underlying power law, we find that upon re-fitting $L_{X,200s}$ and $\alpha_{X,avg,>200s}$, the correlation gets even tighter. Therefore, from here on out, we use the flare-

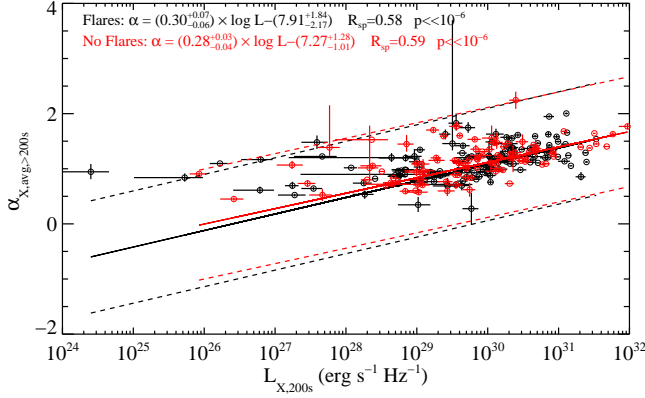


Figure 7. Average decay - luminosity correlation using the sample including steep decay corrections, those only of long duration, and split into those with and without X-ray flares anywhere during the X-ray afterglow. The correlation strengths and regression lines are consistent between the subsamples, with slightly more scatter in the sample with flares. We remove the time intervals of significant flaring and refit the average decay for the rest of this analysis. The solid line indicates the best fit regression, and the dashed lines indicates the 2σ deviation.

removed average decay fits.

3.4. X-ray Plateaus

The complex light curve morphology of X-ray afterglows (Figure 1-3) likely influences the average decay rates. For example, a light curve with an extremely long plateau (e.g. GRB 060729, Grupe et al. 2007, 2010) may have a shallower average decay, whereas GRBs without plateaus would be steeper. Dainotti et al. (2010, 2013) have shown that there is a relationship between the time and flux of the end of the X-ray plateau, which could be another manifestation of the behavior we have found in this study. We test the effect of X-ray plateaus on the average decay-luminosity correlation by separating our sample into those light curves that show plateau behavior (defined as containing segment II in criteria set by Racusin et al. 2009), and those that do not show clear plateaus. Figure 8 demonstrates that the average decay-luminosity correlation is significant in both the sample with and without plateaus. This suggests that the presence of a plateau is not necessarily solely responsible for regulating the average afterglow decay.

3.5. Final Correlation

After correcting for steep decay contamination, filtering on long duration GRBs, and testing for contamination by other light curve morphological features, the final correlation is presented in Figure 9. Much of the scatter in the correlation has been reduced.

However, a small population of shallow average decay, low luminosity GRBs all occupy a parameter space to the left of the best fit regression line. These include a number of “low luminosity” GRBs (Sazonov et al. 2004; Soderberg et al. 2006; Liang et al. 2007) at very low redshifts ($z < 0.3$). The prompt and afterglow emission from these objects tends to be much smoother than their high redshift/high luminosity cousins. Perhaps this represents some sort of asymptotic value of the average slope, with very different X-ray afterglow properties from typical canonical afterglows, perhaps indicative of differ-

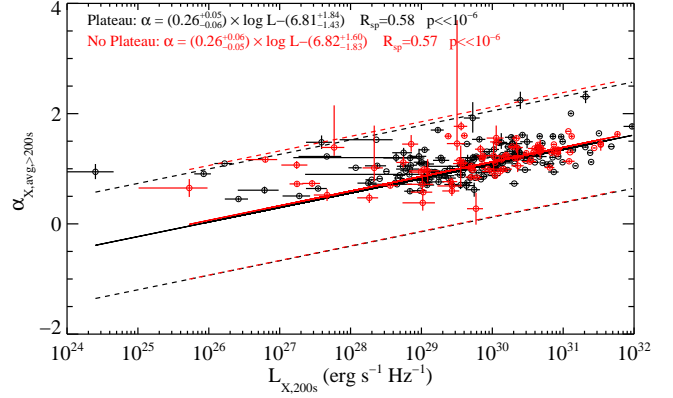


Figure 8. Average decay - luminosity correlation using the sample including steep decay and flare corrections, those only of long duration, and split into those light curves that contain a plateau in their best fit (power-law) models and those that do not. The correlation strengths and regression lines are consistent between the subsamples, suggesting that plateaus do not influence the correlation significantly. Therefore, light curves both with and without plateaus remain in our sample. The solid line indicates the best fit regression, and the dashed lines indicates the 2σ deviation.

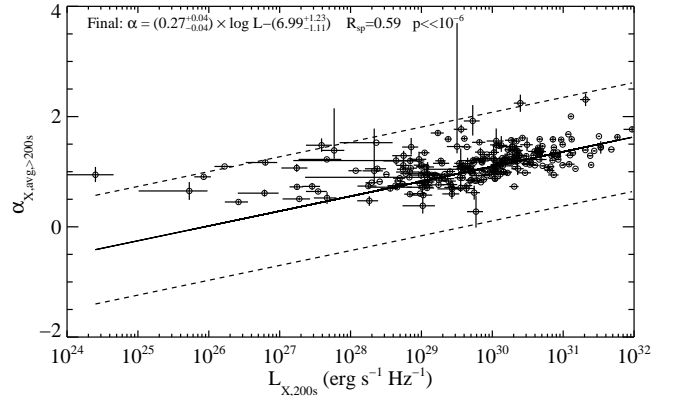


Figure 9. Final average decay - luminosity correlation using the sample that includes steep decay and flares corrections and those only of long duration, with corrections and sub-sample optimization described in §3. The solid line indicates the best fit regression, and the dashed lines indicates the 2σ deviation.

ent jet dynamics or geometry. This small sample of low luminosity GRBs have large errors in $L_{X, 200\text{s}}$, and do not significantly drive the slope or significance of the correlation.

3.6. Individual Segments

The average decay rate of an X-ray light curve characterizes the afterglow differently than the slope of each individual light curve segment. The individual segments are more directly influenced by details of the GRB environment, microphysics, and evolution of the forward shock synchrotron spectrum (Sari et al. 1998; Granot & Sari 2002), as frequently demonstrated via the closure relations (Panaitescu et al. 2006; Zhang et al. 2006; Racusin et al. 2009). To demonstrate that the average decay rate correlation is significantly stronger than any correlation between the slopes of any individual segments, we conduct three tests: 1) we measure the correlation between $L_{x, 200\text{s}}$ and the slope of the light curves at $t_{200\text{s}}$ from

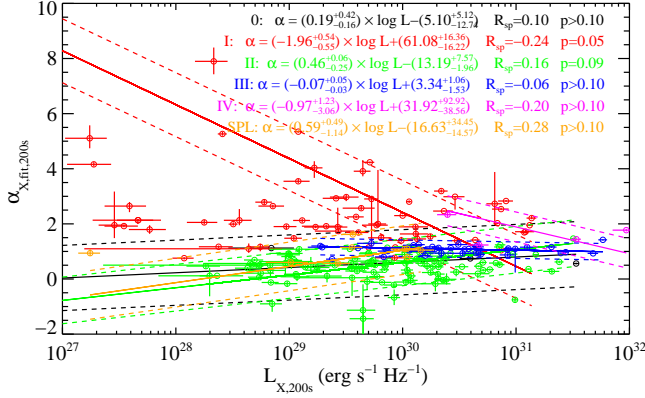


Figure 10. Luminosity - Individual segment decay correlation test, where the temporal slopes and luminosities are interpolated from the best fit (power-law) models (for whichever segment dominates at t_{200s}), rather than the average decay. The roman numerals refer to the segments described in Figure 1 of the best fit (power-law) models, and SPL refers to afterglows consisting of only a single power law. There are no significant correlations present, demonstrating that no individual segment is driving the average decay-luminosity correlation, but rather an average energy output of the afterglow. The solid line indicates the best fit regression, and the dashed lines indicates the 2σ deviation.

the best fit (power-law) models ($\alpha_{X,fit,200s}$) (Figure 10), where each segment refers to those described in Figure 1 ; and 2) we measure the correlation between $L_{X,200s}$ and the slope of the plateau (segment II; if present) even if not observed at t_{200s} ($\alpha_{X,II}$); 3) we measure the correlation between $L_{X,200s}$ and the slope of the normal decay phase (segment III; if present) even if not observed at t_{200s} ($\alpha_{X,III}$). None of the correlations between $L_{X,200s}$ and $\alpha_{X,fit,200s}$ or $\alpha_{X,II}$ or $\alpha_{X,III}$ are significant for any of the segments of the canonical light curve, implying the importance of the average decay measure. All correlation values are given in Table 1.

4. DISCUSSION

The following section demonstrates the robustness of the average decay - luminosity correlation, its uniqueness among other afterglow correlations, and excludes some observational biases.

4.1. Observational Biases

Hypothetically, the longer *Swift* observes a GRB, the more significant the contribution of the normal forward shock decay and post jet-break decay are to the average decay, dragging a fit to the average decay index slightly steeper. For any given canonical light curve (i.e. Figure 1), a jet break within an afterglow is also most likely to be detected if the GRB starts out brighter, allowing the flux post-jet break to be higher relative to the XRT threshold. We test the hypothesis that these effects could be driving the average decay - luminosity correlation.

Additionally, the observing policy of the *Swift* mission has evolved over the last decade further complicating these trends, as *Swift* has transitioned from a primarily GRB mission to an oversubscribed general purpose monitoring and rapid-response observatory, which has reduced the typical time spent on GRB follow-up. In the last few years, GRBs are generally dropped from the observing plan after the first day of observations, unless

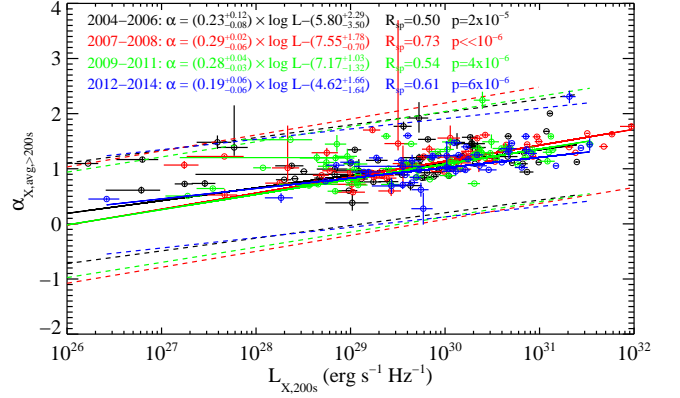


Figure 11. The average decay-luminosity correlation evaluated for our sample split by when the GRBs were detected within the *Swift* mission. The correlation strength is similar throughout the *Swift* mission, demonstrating that the shifting mission policies of reducing GRB observation duration has minimal impact on the correlation strength. The solid line indicates the best fit regression, and the dashed lines indicates the 2σ deviation.

they are especially remarkable and interesting for coordinated follow-up observations.

We evaluate the idea that changes in the duration of observations influenced the average decay - luminosity correlation. We look at the trend of reducing GRB afterglow monitoring duration which has decreased with the years of operation of the *Swift* mission at a rate of $\sim 5 - 10\%$ per year. There is a slight trend of steeper $\alpha_{X,avg>200s}$ with GRBs that were observed for a longer time post trigger, but that may be a real effect as the faster fading GRBs become undetectable sooner after their triggers so are therefore observed for a shorter time. To see the impact of this trend on the average decay-luminosity correlation, we split our sample into roughly equal sized subdivisions by year of their detection (Figure 11). The correlation strength remains significant and similar for each sub-sample. Therefore, the reduction of observation duration has minimal influence on the correlation.

Another potential observational source of the average decay-luminosity correlation is that redshift effects are driving the correlation via GRBs at higher redshift are being observed to have lower initial flux values, and therefore they are less likely to be observed at late times. The longer an X-ray afterglow light curve is observed, the more the average decay is affected by the contributions from the steeper components. In this scenario, the brightest GRBs would be more likely to have observed jet breaks and therefore steeper decay rates, where as the initially fainter GRBs would be less likely to be observed at late times and have shallower decays. We test this hypothesis by conducting Monte Carlo simulations in which we randomize both the redshift and flux normalization of each burst in our sample, then scale each light curve accordingly (new distance, k-correction, t_{200s}). We then fit the average decay rate to the light curve points that occur after the new t_{200s} or end of steep decay, and the points that fall above a fixed conservative XRT threshold of 1×10^{-3} counts s^{-1} . We also extract a new $L_{X,200s}$ from the appropriate quantities. The entire sample is randomized 10^4 times, and for each set of randomizations, we extract $L_{X,200s}$ and $\alpha_{X,avg>200s}$ and measure

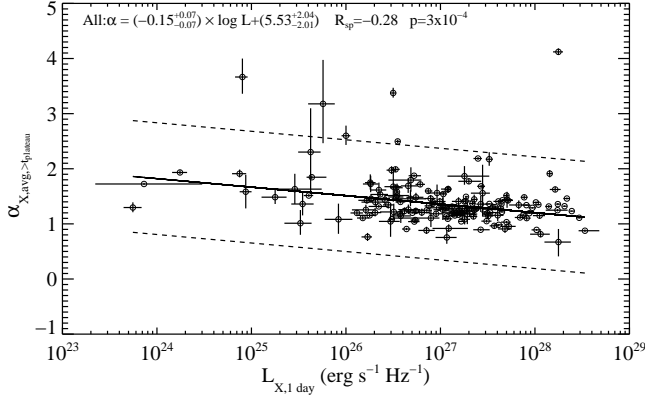


Figure 12. Recreation of the luminosity at 1 day versus average decay after plateau correlation discussed in Boër & Gendre (2000); Gendre & Boër (2005); Gendre et al. (2008); Bardho et al. (2015). We find a correlation in the opposite direction to that of these authors, which makes sense in the context of the correlation discussed in this paper, and demonstrates why measuring the correlation at early times is more robust. The solid line indicates the best fit regression, and the dashed lines indicates the 2σ deviation.

the correlation strength in the same manner as in §3. Of the 10^4 simulations, none of the R_{sp} coefficients are anywhere near the value from our measured correlations.

4.2. Robustness of Average Decay-Luminosity Correlation Compared to Other GRB Correlations

There are other correlations in the literature between various afterglow quantities, which we recreate with our sample and measurements for comparison, validation, and discussion of whether or not these correlations are measurement of the same energy dissipation mechanism.

Dainotti et al. (2010, 2013) describe a correlation between the time and luminosity of X-ray afterglows at the end of their plateaus. We reproduce this measurement, confirming that the plateau time-luminosity correlation is very significant in our sample, with $R_{sp} = -0.71$ ($p = 1.89 \times 10^{-26}$). While Dainotti’s correlation has a similar or slightly stronger significance compared to the average decay - luminosity, it is only applicable to the $\sim 60\%$ of GRBs with a plateau segment, therefore the average decay - luminosity correlation is a more general description of afterglow behavior.

Boër & Gendre (2000); Gendre & Boër (2005); Gendre et al. (2008); Bardho et al. (2015) describe early measurements of BeppoSAX and the first years of XRT afterglow observations, and an apparent clustering in luminosity space for which subsets had on average different decay rates, suggesting that the more luminous GRBs decay faster than the less luminous ones. However, this correlation became non-significant as a larger sample was accumulated (Gendre et al. 2008; Bardho et al. 2015). When we reconstruct their measurement, the decay rate after the end of the plateau versus the luminosity at 1 day, with our larger sample (Figure 12), we find that there is a correlation with $R_{sp} = -0.28$ ($p = 3.04 \times 10^{-4}$). However, we note that this correlation is actually going in the opposite direction as previously claimed, and in the opposite direction of the average decay-luminosity correlation (at t_{200}). This can be easily reconciled by noting that as the more luminous afterglows decay faster (early on), at some later point (~ 1 day), the trend intersects,

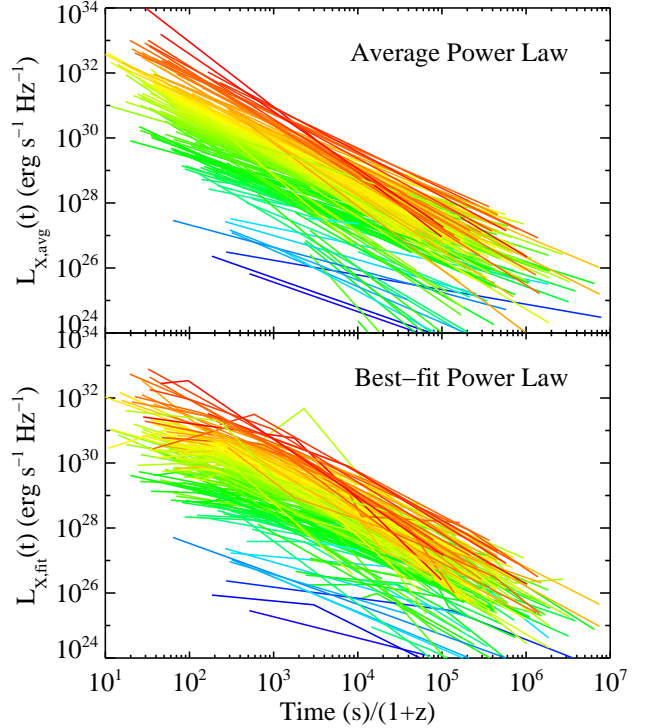


Figure 13. The average power-law models to each long GRB afterglow (top panel) and best fit (power-law) models (bottom panel) colored by $L_{X,avg,200s}$ demonstrates the average decay - luminosity correlation qualitatively. The color distinction is very clear at early times, and gets more mixed together at later times when the faster decay afterglows are no longer the brightest.

and afterwards on average, the faster decaying afterglows have become the fainter ones (Figure 13). We quantify this by measuring the spread of the luminosity distribution of light curves as a function of time for both the best fit (power-law) models and average power-law models to our light curves (Figure 14). In both cases, though more clearly in the average power-law models, the spread decreases with time initially until $\sim 10^4$ s and reverses the trend increasing afterwards.

4.3. Origin of the Average Decay - Luminosity Correlation

As described in Oates et al. (2012, 2015), the physical origin of the correlation is somewhat uncertain, though Oates et al. (2015) explored the expectations for the luminosity - average decay correlation from the standard afterglow forward shock model (Sari et al. 1998; Zhang et al. 2007) by performing Monte Carlo simulations drawing randomly from distributions of microphysical parameters: the kinetic energy of the outflow (E_K), the fraction of energy in the electric (ϵ_e) and magnetic fields (ϵ_B), the environmental density (n), and the electron spectral index (p). Oates et al. (2015) used the theoretical relationships (the closure relations; Zhang et al. (2006); Racusin et al. (2009); Gao et al. (2013)) between these parameters to derive the amplitude and shape of afterglow spectra and light curves, which in turn provided values for $L_{X,avg,200s}$ and $\alpha_{X,avg,>200s}$ for a sample the same size as their dataset. They repeated this exercise for 10^4 iterations, and determined that despite the

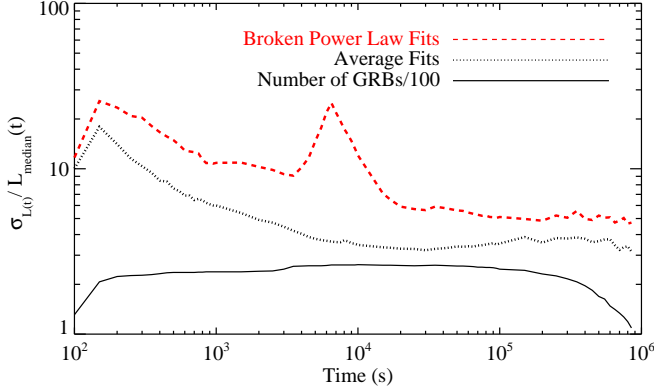


Figure 14. The time averaged spread of the light curve fits (Figure 13), measured as the standard deviation ($\sigma_{L(t)}$) of the luminosity distribution divided by the median luminosity as a function of time ($L_{median}(t)$). The solid black curve indicates the scaled number of GRBs observed at those timescales used in the spread measurement, which drops off < 200 s and $> 3 \times 10^5$ s timescales, making them noisy. The spread measurements are interpolated from the average (black dotted) and best fit (power-law) models (red dashed). This parameterization demonstrates that the distribution of luminosities narrows and then widens with time, consistent with the picture that the fastest fading afterglows begin luminous and around $\sim 10^4$ s they converge, and becoming the least luminous. This behavior is most obvious in the average power-law models, where as the best fit (power-law) models are muddled by the various durations of plateaus, causing the spike around 7×10^4 s.

simulated GRBs having similar X-ray-optical behavior, the Spearman rank coefficients for the optical and X-ray luminosity-average decay correlations were inconsistent with the observed values at a significance of $\gtrsim 4\sigma$. The implication is that the observed correlations are much stronger than what is expected from theoretical models.

The average decay-luminosity correlation could be the result of viewing geometry. As van Eerten et al. (2010); van Eerten & MacFadyen (2011); Ryan et al. (2015) have shown with their relativistic hydrodynamic simulations, jets viewed further away from the jet axis (but inside the jet cone) show later jet breaks, and fainter overall afterglow emission due to the role of jet spreading. This would suggest that those afterglows that start out bright and fade sooner might be viewed more on-axis than those that start out fainter and fade slower. We tested this by searching for a correlation between our early time luminosity, average decay, and the off-axis observer angle for the GRBs in common with the sample from Ryan et al. (2015). Unfortunately, we found no significant correlation with the fractional observer angle. Note that these simulations do not include a mechanism for X-ray plateaus, and only fit light curves after this phase, for which good measurements are only available on a small subset of the sample (Ryan et al. 2015). This does not rule out jet geometry as the cause of the correlation, but does suggest that it might be only one component of the mechanism that affects the average GRB afterglow decay rate.

Another possible origin for the average decay-luminosity correlation could be related the relationship between the theoretical Synchrotron cooling timescale and the inverse of the strength of the magnetic field and the bulk Lorentz factor (Γ): $t_{sync}(\nu) \sim (B^3\Gamma)^{-0.5}$ (Piran

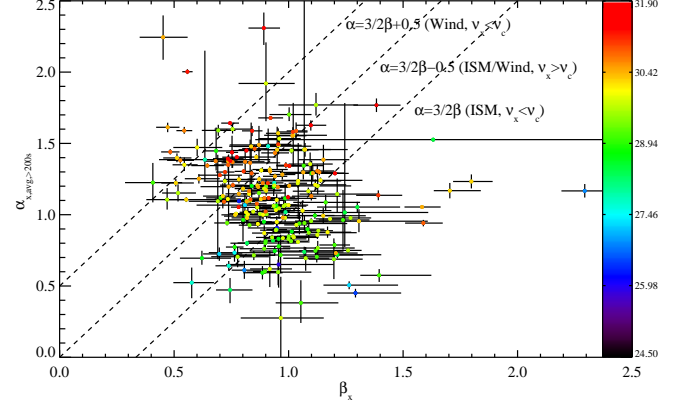


Figure 15. The average temporal decay ($\alpha_{avg,x,>200s}$) and average spectral energy index (β_x) are compared with $\log L_{x,200s}$ (color scale), demonstrating consistency and trends with the closure relations (dashed lines). The high luminosity (redder) points are roughly consistent with Wind-like environments.

2004, eq. 19). If t_{sync} is a proxy for the average decay rate (i.e. shorter cooling timescale causes steeper average decay), then it should scale with either large magnetic fields or large Γ , or both. The cooling timescale is another way to parameterize the cooling frequency ν_c , which should be low (perhaps below the X-ray band) if Γ is very high, which for a constant density ISM environment would cause the X-ray flux to be steep. Liang et al. (2010) and Ghirlanda et al. (2012) have shown that there is a correlation between Γ and $E_{\gamma,iso}$ or $L_{\gamma,iso}$, and Gehrels et al. (2008) and Nysewander et al. (2009) have shown a correlation between $E_{\gamma,iso}$ and the afterglow luminosity, therefore it follows that the luminosity and average decay rate should be linked.

Yet another possible physical origin for the average decay-luminosity correlation could be rooted in the circumburst environment. We look at $\alpha_{x,avg,>200s}$ and L_{200s} in the context of the closure relations (Panaitescu et al. 2006; Zhang et al. 2006; Racusin et al. 2009) adding the spectral energy index (β_x) for the standard forward shock (Figure 15). The highest luminosity GRBs tend toward the lines demarcating the R^{-2} wind environment with the X-ray band (ν_x) below the synchrotron cooling frequency (ν_c), and the line showing either a constant density ISM or a Wind profile with the X-ray band above the cooling frequency, and away from the ISM profile with $\nu_x < \nu_c$. The ambiguity in the $\nu_x > \nu_c$ cases prohibits us from making a strong statement on the role of circumburst environment, but it may be another possible contribution in that the initially brightest GRB afterglows may be more likely to live in Wind-like environments (see also De Pasquale et al. 2013).

Based upon the optical correlation (Oates et al. 2012, 2015) alone, one could hypothesize that the most energetic GRBs show a bright short-lived reverse shock that would cause the average afterglow to be steeper. However, the presence of the X-ray correlation rules out this idea, as the reverse shock is expected to produce strong emission in the optical band, but not the X-ray band (Sari & Piran 1999).

5. CONCLUSIONS

In this paper, we show that there is a significant correlation between early GRB X-ray afterglow luminosity and the average decay rate of that afterglow, suggestive of some mechanism that moderates the energy dissipation in GRB jets. This mechanism could be related to the interaction with the circumburst environment, physical parameters of the jet, or geometrical effects. The correlation is undoubtedly significant, and complementary to other afterglow correlations demonstrated in the literature. It is also only present in the average decay and not in the individual segments of the canonical afterglow light curve. We argue that the average decay - luminosity correlation is more robust than other afterglow correlations as the decay rate is redshift independent, and it can be applied to all long GRBs independent of their individual light curve morphologies (e.g. with and without plateaus).

Although the precise origin of the correlation remains unclear, GRB jet propagation model and numerical simulations should strive to reproduce this observational feature. The role of geometry and viewing angle within the jet surely has a significant impact on the observed emission, and disentangling that from intrinsic physics remains difficult.

Oates et al. (2015) compared the UV/optical and X-ray average decay - luminosity correlations, and explored many correlations with prompt emission param-

eters (T_{90} , $E_{\gamma,iso}$), and determined that a correlation as significant as the observed one could not be predicted with the fireball model framework.

As redshift is a fundamental quantity in the luminosity measurement, and the average decay is mostly redshift independent, the correlation can be inverted to roughly estimate redshifts. We attempt this redshift estimation, but the scatter between measured redshift and actual redshift deviate by $\Delta z \sim 2$ (1σ). Therefore, the intrinsic scatter in the average decay-luminosity correlation prevents estimated redshifts with errors small enough to be of any use in GRB physical parameter estimation or cosmology. Perhaps more detailed work on this topic could improve this estimation technique, which could be explored in a future paper.

ACKNOWLEDGEMENTS

The authors thank the anonymous referee for helpful comments, as well as Brad Cenko and Raffaella Margutti for useful discussions. This work made use of data supplied by the UK *Swift* Science Data Centre at the University of Leicester. SRO acknowledges the support of the Spanish Ministry, Project Number AYA2012-39727-C03-01. MDP acknowledges the support of the UK Space Agency. DK acknowledges the support of the NASA Postdoctoral Program.

GRB	z	z reference	T_{90} (s)	$\alpha_{X,avg,>200s}$	$L_{X,200s}$ (erg cm ⁻² Hz ⁻¹)	Steep Decay Contaminated	Plateau	Flares
GRB050126	1.29	Berger et al. (2005b)	48.0	0.96 ± 0.21	$(1.22 \pm 0.55) \times 10^{29}$	n	n	n
GRB050315	1.95	Berger et al. (2005a)	95.4	0.60 ± 0.02	$(9.59 \pm 2.19) \times 10^{28}$	n	y	n
GRB050319	3.24	Fynbo et al. (2009b)	151.6	0.84 ± 0.02	$(5.72 \pm 1.01) \times 10^{29}$	n	y	n
GRB050401	2.90	Fynbo et al. (2009b)	33.3	1.09 ± 0.02	$(6.63 \pm 0.87) \times 10^{30}$	n	y	n
GRB050416A	0.65	Soderberg et al. (2007)	6.7	0.83 ± 0.01	$(4.69 \pm 0.56) \times 10^{28}$	n	y	n
GRB050502B	5.20	Afonso et al. (2011)	17.7	0.87 ± 0.05	$(1.10 \pm 0.12) \times 10^{30}$	n	n	y
GRB050525A	0.61	Foley et al. (2005a)	8.8	1.53 ± 0.04	$(6.58 \pm 1.40) \times 10^{29}$	n	y	n
GRB050724	0.26	Prochaska et al. (2005)	98.7	0.72 ± 0.05	$(1.75 \pm 0.39) \times 10^{27}$	n	n	y
GRB050730	3.97	Fynbo et al. (2009b)	154.6	2.00 ± 0.02	$(1.29 \pm 0.07) \times 10^{31}$	n	y	y
GRB050801	1.38	Oates et al. (2009)	19.6	1.15 ± 0.04	$(1.95 \pm 0.52) \times 10^{29}$	n	y	n
GRB050802	1.71	Fynbo et al. (2009b)	27.5	1.18 ± 0.01	$(1.41 \pm 0.11) \times 10^{30}$	n	y	y
GRB050814	5.30	Jakobsson et al. (2006a)	142.9	0.94 ± 0.02	$(8.42^{+1.06}_{-1.02}) \times 10^{29}$	n	y	y
GRB050819	2.50	Krühler et al. (2012)	37.7	0.38 ± 0.16	$(1.04 \pm 0.51) \times 10^{29}$	n	n	y
GRB050820A	2.61	Fynbo et al. (2009b)	240.8	1.22 ± 0.01	$(4.60 \pm 1.23) \times 10^{30}$	n	y	y
GRB050822	1.43	Hjorth et al. (2012)	104.3	0.81 ± 0.02	$(1.30 \pm 0.22) \times 10^{29}$	n	y	y
GRB050826	0.30	Mirabal et al. (2007)	29.6	1.05 ± 0.04	$(2.38 \pm 0.79) \times 10^{28}$	n	y	n
GRB050904	6.29	Kawai et al. (2006)	181.6	1.29 ± 0.03	$(6.85 \pm 0.53) \times 10^{30}$	n	n	y
GRB050908	3.34	Fynbo et al. (2009b)	18.3	1.23 ± 0.05	$(1.52 \pm 0.38) \times 10^{30}$	n	y	y
GRB050915A	2.53	Krühler et al. (2012)	53.4	1.20 ± 0.07	$(5.32 \pm 1.86) \times 10^{29}$	n	y	y
GRB050922C	2.20	Fynbo et al. (2009b)	4.6	1.30 ± 0.02	$(3.82 \pm 0.37) \times 10^{30}$	n	y	n
GRB051001	2.43	Krühler et al. (2012)	190.3	0.77 ± 0.06	$(2.59 \pm 0.62) \times 10^{29}$	y	n	n
GRB051006	1.06	Hjorth et al. (2012)	35.4	1.77 ± 0.08	$(3.64 \pm 0.79) \times 10^{29}$	n	n	n
GRB051016B	0.94	Soderberg et al. (2005)	4.0	0.80 ± 0.02	$(1.99 \pm 0.37) \times 10^{28}$	n	y	n
GRB051109A	2.35	Quimby et al. (2005)	36.2	1.19 ± 0.01	$(3.34 \pm 0.45) \times 10^{30}$	n	y	n
GRB051109B	0.08	Perley et al. (2006)	15.7	0.91 ± 0.03	$(8.47 \pm 2.24) \times 10^{25}$	n	y	n
GRB051117B	0.48	Hjorth et al. (2012)	9.0	$1.39^{+0.76}_{-0.15}$	$(5.87^{+2.30}_{-2.02}) \times 10^{27}$	n	n	n
GRB051221A	0.55	Berger & Soderberg (2005)	1.4	0.94 ± 0.02	$(6.61 \pm 2.07) \times 10^{27}$	n	y	y
GRB051227	0.80	Foley et al. (2005b)	115.4	1.48 ± 0.12	$(3.90 \pm 1.56) \times 10^{27}$	y	y	y
GRB060108	2.70	Melandri et al. (2006)	14.2	0.76 ± 0.03	$(1.74 \pm 0.36) \times 10^{29}$	n	y	y
GRB060111A	2.32	Perley Host ⁸	13.2	0.84 ± 0.03	$(6.06 \pm 1.09) \times 10^{29}$	n	n	y
GRB060115	3.53	Fynbo et al. (2009b)	139.1	0.86 ± 0.03	$(7.59 \pm 0.96) \times 10^{29}$	n	y	y
GRB060124	2.30	Fynbo et al. (2009b)	13.4	1.12 ± 0.01	$(9.79 \pm 0.63) \times 10^{30}$	n	y	y
GRB060202	0.78	Perley et al. (2013)	192.9	0.94 ± 0.02	$(7.38 \pm 1.24) \times 10^{30}$	n	y	y
GRB060206	4.05	Fynbo et al. (2009b)	7.6	1.24 ± 0.02	$(8.49 \pm 2.82) \times 10^{29}$	y	y	n
GRB060210	3.91	Fynbo et al. (2009b)	288.0	1.12 ± 0.02	$(2.48 \pm 0.13) \times 10^{31}$	n	y	y

Continued on next page

⁸ <http://www.astro.caltech.edu/grbhosts/redshifts.html>

GRB	z	z reference	T_{90} (s)	$\alpha_{X,avg,>200s}$	$L_{X,200s}$ (erg cm ⁻² Hz ⁻¹)	Steep Decay Contaminated	Plateau	Flares
GRB060218	0.03	Mirabal & Halpern (2006)	80.0	1.17 ± 0.05	$(6.27 \pm 2.95) \times 10^{26}$	y	y	y
GRB060223A	4.41	Berger et al. (2006)	11.3	$1.92^{+0.29}_{-0.26}$	$(5.30 \pm 1.34) \times 10^{29}$	n	y	y
GRB060319	1.17	Perley et al. (2013)	10.3	0.99 ± 0.02	$(6.83 \pm 2.44) \times 10^{28}$	n	y	y
GRB060418	1.49	Dupree et al. (2006)	109.1	1.40 ± 0.02	$(1.92 \pm 0.25) \times 10^{30}$	n	y	y
GRB060502A	1.51	Fynbo et al. (2009b)	508.1	0.89 ± 0.02	$(3.49 \pm 0.56) \times 10^{29}$	n	y	n
GRB060510A	1.20	Oates et al. (2012)	20.1	1.01 ± 0.01	$(1.19 \pm 0.11) \times 10^{30}$	n	y	n
GRB060510B	4.94	Price (2006)	262.9	0.69 ± 0.09	$(4.31 \pm 1.35) \times 10^{29}$	n	y	y
GRB060512	2.10	Fynbo et al. (2009b)	8.4	1.17 ± 0.05	$(1.35 \pm 0.26) \times 10^{30}$	n	n	y
GRB060522	5.11	Cenko et al. (2006)	69.1	1.39 ± 0.10	$(2.20 \pm 0.50) \times 10^{30}$	n	y	y
GRB060526	3.22	Fynbo et al. (2009b)	298.0	1.00 ± 0.03	$(8.61 \pm 1.68) \times 10^{29}$	n	y	y
GRB060604	2.14	Krühler et al. (2012)	96.0	0.90 ± 0.02	$(6.77 \pm 6.54) \times 10^{28}$	n	y	y
GRB060605	3.78	Ferrero et al. (2009)	580.9	1.57 ± 0.04	$(1.85 \pm 0.34) \times 10^{30}$	n	y	y
GRB060607A	3.07	Fynbo et al. (2009b)	103.0	1.59 ± 0.03	$(4.66 \pm 0.41) \times 10^{30}$	n	y	y
GRB060614	0.13	Della Valle et al. (2006)	109.1	1.09 ± 0.02	$(1.67 \pm 0.47) \times 10^{26}$	y	y	y
GRB060707	3.42	Fynbo et al. (2009b)	66.6	0.93 ± 0.02	$(6.46 \pm 1.50) \times 10^{29}$	y	y	y
GRB060708	1.92	Fynbo et al. (2009b)	10.0	1.16 ± 0.03	$(5.50 \pm 0.65) \times 10^{29}$	n	y	n
GRB060714	2.71	Fynbo et al. (2009b)	116.1	1.03 ± 0.02	$(1.10 \pm 0.14) \times 10^{30}$	n	y	y
GRB060719	1.53	Krühler et al. (2012)	66.9	0.98 ± 0.02	$(3.89 \pm 0.61) \times 10^{29}$	n	y	y
GRB060729	0.54	Fynbo et al. (2009b)	113.0	0.82 ± 0.01	$(2.58 \pm 0.23) \times 10^{28}$	n	y	y
GRB060814	1.92	Krühler et al. (2012)	145.1	1.07 ± 0.01	$(1.00 \pm 0.16) \times 10^{30}$	n	y	y
GRB060904B	0.70	Fynbo et al. (2009b)	190.0	1.34 ± 0.04	$(1.11 \pm 0.19) \times 10^{29}$	n	y	y
GRB060906	3.69	Fynbo et al. (2009b)	44.6	1.06 ± 0.04	$(3.96 \pm 0.84) \times 10^{29}$	n	y	y
GRB060908	1.88	Fynbo et al. (2009b)	19.3	1.46 ± 0.05	$(1.90 \pm 0.31) \times 10^{30}$	n	y	n
GRB060912A	0.94	Jakobsson et al. (2006b)	5.0	1.10 ± 0.03	$(9.92 \pm 1.42) \times 10^{28}$	n	y	n
GRB060923A	2.80	Perley et al. (2013)	58.5	1.10 ± 0.02	$(4.47 \pm 1.26) \times 10^{29}$	n	y	n
GRB060926	3.20	Fynbo et al. (2009b)	8.8	$1.46^{+0.16}_{-0.14}$	$(1.94 \pm 0.70) \times 10^{30}$	n	y	y
GRB060927	5.47	Ruiz-Velasco et al. (2007)	22.4	$1.48^{+0.17}_{-0.12}$	$(1.34 \pm 0.29) \times 10^{30}$	n	y	n
GRB061006	0.44	Berger et al. (2007c)	129.8	0.73 ± 0.06	$(2.87^{+0.84}_{-0.79}) \times 10^{27}$	n	n	n
GRB061007	1.26	Fynbo et al. (2009b)	75.7	1.68 ± 0.01	$(1.18 \pm 0.09) \times 10^{31}$	n	n	n
GRB061021	0.35	Fynbo et al. (2009b)	47.8	0.95 ± 0.01	$(3.21 \pm 0.29) \times 10^{28}$	n	y	n
GRB061110A	0.76	Fynbo et al. (2009b)	44.5	0.61 ± 0.07	$(6.11 \pm 3.55) \times 10^{26}$	y	y	y
GRB061121	1.31	Fynbo et al. (2009b)	81.2	1.09 ± 0.01	$(2.07 \pm 0.13) \times 10^{30}$	n	y	y
GRB061222A	2.09	Perley et al. (2009c)	96.0	1.11 ± 0.01	$(5.12 \pm 0.36) \times 10^{30}$	n	y	y
GRB070103	2.62	Krühler et al. (2012)	18.4	1.21 ± 0.04	$(1.07 \pm 0.23) \times 10^{30}$	n	y	y
GRB070110	2.35	Fynbo et al. (2009b)	88.4	1.22 ± 0.03	$(5.95 \pm 0.87) \times 10^{29}$	n	y	y
GRB070129	2.34	Krühler et al. (2012)	459.7	0.96 ± 0.02	$(2.12 \pm 0.83) \times 10^{29}$	y	y	y
GRB070208	1.16	Cucchiara et al. (2007b)	64.0	1.29 ± 0.09	$(5.61 \pm 1.74) \times 10^{28}$	n	y	y
GRB070306	1.50	Jaunsen et al. (2008)	209.2	0.93 ± 0.02	$(1.66 \pm 0.30) \times 10^{29}$	n	y	y
GRB070318	0.84	Chen et al. (2007)	130.4	1.05 ± 0.04	$(5.02 \pm 0.43) \times 10^{29}$	n	y	y
GRB070411	2.95	Jakobsson et al. (2007a)	102.0	1.13 ± 0.03	$(3.38 \pm 0.78) \times 10^{30}$	n	y	n
GRB070419A	0.97	Cenko et al. (2007)	160.0	$1.46^{+2.24}_{-0.12}$	$(3.18 \pm 0.90) \times 10^{29}$	n	n	y
GRB070419B	1.96	Krühler et al. (2012)	238.0	1.44 ± 0.02	$(7.39 \pm 0.58) \times 10^{30}$	n	y	y
GRB070506	2.31	Thoene et al. (2007a)	6.0	0.60 ± 0.09	$(2.69 \pm 0.73) \times 10^{29}$	n	n	n
GRB070508	3.00	Jakobsson et al. (2007b)	20.9	1.39 ± 0.01	$(2.05 \pm 0.22) \times 10^{31}$	n	y	n
GRB070518	1.16	Perley Host ⁸	5.5	0.74 ± 0.04	$(1.78 \pm 0.54) \times 10^{28}$	y	y	y
GRB070521	1.35	Perley et al. (2013)	38.6	1.32 ± 0.02	$(1.76 \pm 0.29) \times 10^{30}$	n	y	y
GRB070529	2.50	Berger et al. (2007a)	108.9	1.20 ± 0.03	$(1.51 \pm 0.25) \times 10^{30}$	n	y	n
GRB070714A	1.58	Perley Host ⁸	3.0	0.87 ± 0.06	$(2.15 \pm 0.74) \times 10^{29}$	n	y	y
GRB070714B	0.92	Berger (2009)	65.6	1.70 ± 0.05	$(1.71 \pm 0.36) \times 10^{29}$	y	y	n
GRB070721B	3.63	Fynbo et al. (2009b)	336.9	1.61 ± 0.03	$(2.66 \pm 0.33) \times 10^{30}$	n	y	y
GRB070724A	0.46	Cucchiara et al. (2007c)	0.4	1.26 ± 0.11	$(1.06 \pm 0.57) \times 10^{27}$	y	y	y
GRB070802	2.45	Fynbo et al. (2009b)	15.8	0.80 ± 0.04	$(1.15 \pm 0.25) \times 10^{29}$	n	y	n
GRB070809	0.22	Perley et al. (2008)	1.3	0.52 ± 0.05	$(4.23 \pm 1.14) \times 10^{26}$	n	y	n
GRB070810A	2.17	Thoene et al. (2007b)	9.0	1.36 ± 0.08	$(6.81 \pm 1.11) \times 10^{29}$	n	y	n
GRB071020	2.14	Fynbo et al. (2009b)	4.3	1.22 ± 0.03	$(1.83 \pm 0.27) \times 10^{30}$	n	y	y
GRB071021	2.45	Krühler et al. (2012)	228.7	0.83 ± 0.03	$(2.41 \pm 0.65) \times 10^{29}$	n	y	y
GRB071025	5.20	Fynbo et al. (2009b)	241.3	1.63 ± 0.04	$(5.83 \pm 0.52) \times 10^{31}$	n	y	n
GRB071031	2.69	Fynbo et al. (2009b)	180.6	1.13 ± 0.09	$(1.31 \pm 0.37) \times 10^{30}$	n	y	y
GRB071122	1.14	Cucchiara et al. (2007a)	71.4	3.10 ± 0.33	$(1.26 \pm 0.29) \times 10^{29}$	y	n	y
GRB071227	0.38	Berger (2009)	142.5	1.07 ± 0.07	$(1.74^{+0.72}_{-0.68}) \times 10^{27}$	n	n	n
GRB080123	0.50	Leibler & Berger (2010)	114.9	$1.02^{+0.77}_{-0.24}$	$(2.16 \pm 0.70) \times 10^{28}$	n	n	n
GRB080207	2.09	Hjorth et al. (2012)	292.5	1.77 ± 0.05	$(9.38 \pm 2.27) \times 10^{31}$	n	y	n
GRB080210	2.64	Fynbo et al. (2009b)	42.3	1.30 ± 0.05	$(2.20 \pm 0.27) \times 10^{30}$	n	y	y
GRB080310	2.42	Fynbo et al. (2009b)	363.2	1.07 ± 0.03	$(4.08 \pm 0.92) \times 10^{29}$	n	y	y
GRB080319B	0.94	Fynbo et al. (2009b)	124.9	1.64 ± 0.01	$(3.20 \pm 0.13) \times 10^{31}$	n	y	n
GRB080319C	1.95	Fynbo et al. (2009b)	29.6	1.38 ± 0.03	$(4.43 \pm 0.53) \times 10^{30}$	n	y	y
GRB080325	1.78	Perley et al. (2013)	166.7	0.99 ± 0.06	$(1.44 \pm 0.45) \times 10^{30}$	n	n	y
GRB080413A	2.43	Fynbo et al. (2009b)	46.4	1.56 ± 0.23	$(1.14 \pm 0.31) \times 10^{30}$	n	n	n

Continued on next page

GRB	z	z reference	T_{90} (s)	$\alpha_{X,avg,>200s}$	$L_{X,200s}$ (erg cm ⁻² Hz ⁻¹)	Steep Decay Contaminated	Plateau	Flares
GRB080413B	1.10	Fynbo et al. (2009b)	8.0	1.02 ± 0.01	$(7.12 \pm 0.51) \times 10^{29}$	n	y	n
GRB080430	0.77	Cucchiara & Fox (2008)	13.9	0.78 ± 0.01	$(5.39 \pm 0.52) \times 10^{28}$	n	y	n
GRB080517	0.09	Stanway et al. (2015)	64.5	0.65 ± 0.16	$(5.31 \pm 4.29) \times 10^{25}$	y	n	y
GRB080520	1.54	Fynbo et al. (2009b)	3.3	0.94 ± 0.08	$(9.90^{+3.21}_{-3.19}) \times 10^{28}$	n	n	n
GRB080603B	2.69	Fynbo et al. (2009b)	59.1	$1.20^{+0.23}_{-0.26}$	$(2.28 \pm 0.52) \times 10^{30}$	n	n	n
GRB080604	1.42	Wiersema et al. (2008)	77.6	0.52 ± 0.11	$(4.66 \pm 1.65) \times 10^{27}$	y	n	n
GRB080605	1.64	Fynbo et al. (2009b)	18.1	1.34 ± 0.02	$(4.65 \pm 0.55) \times 10^{30}$	n	y	n
GRB080607	3.04	Fynbo et al. (2009b)	79.0	1.49 ± 0.02	$(9.83 \pm 0.95) \times 10^{30}$	n	y	y
GRB080707	1.23	Fynbo et al. (2009b)	30.2	0.75 ± 0.03	$(4.29 \pm 0.97) \times 10^{28}$	n	y	n
GRB080721	2.59	Fynbo et al. (2009b)	159.0	1.40 ± 0.01	$(4.78 \pm 0.51) \times 10^{31}$	n	y	n
GRB080804	2.20	Fynbo et al. (2009b)	37.9	1.11 ± 0.02	$(1.09 \pm 0.08) \times 10^{30}$	n	n	n
GRB080805	1.50	Fynbo et al. (2009b)	106.6	0.95 ± 0.04	$(9.74^{+2.61}_{-2.59}) \times 10^{29}$	n	n	y
GRB080810	3.35	Fynbo et al. (2009b)	107.7	1.58 ± 0.03	$(9.37 \pm 0.91) \times 10^{30}$	n	y	y
GRB080905A	0.12	Rowlinson et al. (2010)	1.0	2.75 ± 0.18	$(2.57 \pm 0.76) \times 10^{27}$	n	y	n
GRB080905B	2.37	Fynbo et al. (2009b)	120.9	1.15 ± 0.02	$(2.97 \pm 0.34) \times 10^{30}$	n	y	n
GRB080906	2.10	Holland (2008)	148.2	1.11 ± 0.02	$(1.40^{+0.48}_{-0.43}) \times 10^{30}$	n	y	y
GRB080913	6.70	Fynbo et al. (2008)	7.5	$1.09^{+0.33}_{-0.41}$	$(3.58^{+0.81}_{-0.79}) \times 10^{29}$	n	n	y
GRB080916A	0.69	Fynbo et al. (2009b)	61.3	0.96 ± 0.02	$(6.02 \pm 1.00) \times 10^{28}$	n	y	y
GRB080928	1.69	Fynbo et al. (2009b)	233.7	1.55 ± 0.04	$(2.19 \pm 0.30) \times 10^{30}$	n	y	y
GRB081007	0.53	Berger et al. (2008b)	9.7	0.88 ± 0.02	$(4.94 \pm 0.95) \times 10^{28}$	n	y	y
GRB081008	1.97	Cucchiara et al. (2008a)	187.8	1.25 ± 0.02	$(1.58 \pm 0.18) \times 10^{30}$	n	y	y
GRB081028A	3.04	Berger et al. (2008a)	284.4	1.22 ± 0.03	$(4.62 \pm 2.77) \times 10^{27}$	y	y	y
GRB081109	0.98	Krühler et al. (2011b)	221.5	1.17 ± 0.02	$(7.17 \pm 0.65) \times 10^{29}$	n	y	n
GRB081118	2.58	D'Elia et al. (2008)	53.4	0.58 ± 0.05	$(1.06 \pm 0.36) \times 10^{29}$	n	n	n
GRB081203A	2.05	Landsman et al. (2008)	223.0	1.43 ± 0.02	$(4.44 \pm 0.37) \times 10^{30}$	n	y	n
GRB081221	2.26	Salvaterra et al. (2012)	33.9	1.29 ± 0.01	$(2.40 \pm 0.22) \times 10^{31}$	n	y	y
GRB081222	2.77	Cucchiara et al. (2008b)	33.0	1.22 ± 0.01	$(8.53 \pm 0.70) \times 10^{30}$	n	y	n
GRB081228	3.40	Afonso et al. (2008)	3.0	0.72 ± 0.14	$(1.03^{+0.43}_{-0.41}) \times 10^{29}$	n	n	n
GRB081230	2.00	Krühler et al. (2011a)	60.7	0.85 ± 0.03	$(1.77 \pm 0.49) \times 10^{29}$	n	y	y
GRB090102	1.55	de Ugarte Postigo et al. (2009a)	24.7	1.38 ± 0.01	$(4.88 \pm 0.43) \times 10^{30}$	n	y	n
GRB090113	1.75	Krühler et al. (2012)	9.1	1.29 ± 0.06	$(2.44 \pm 0.54) \times 10^{30}$	n	y	n
GRB090205	4.65	Fugazza et al. (2009)	8.8	1.10 ± 0.04	$(1.17 \pm 0.18) \times 10^{30}$	n	y	n
GRB090401B	3.10	Oates et al. (2012)	186.5	1.45 ± 0.01	$(3.40 \pm 0.33) \times 10^{31}$	n	y	n
GRB090407	1.45	Krühler et al. (2012)	315.5	0.79 ± 0.02	$(9.43 \pm 2.15) \times 10^{28}$	n	y	y
GRB090417B	0.34	Berger & Fox (2009)	266.9	1.45 ± 0.02	$(4.38 \pm 0.69) \times 10^{29}$	n	y	y
GRB090418A	1.61	Chornock et al. (2009c)	56.3	1.27 ± 0.02	$(2.07 \pm 0.22) \times 10^{30}$	n	y	n
GRB090423	8.26	Tanvir et al. (2009)	10.3	1.37 ± 0.04	$(2.28 \pm 0.32) \times 10^{30}$	n	y	y
GRB090424	0.54	Chornock et al. (2009a)	49.5	1.11 ± 0.01	$(1.32 \pm 0.10) \times 10^{30}$	n	y	n
GRB090426	2.61	Levesque et al. (2009)	1.2	1.04 ± 0.05	$(4.63 \pm 0.68) \times 10^{29}$	n	y	n
GRB090429B	9.20	Cucchiara et al. (2011c)	5.6	1.49 ± 0.13	$(3.09 \pm 0.63) \times 10^{30}$	n	y	n
GRB090510	0.90	Rau et al. (2009)	5.7	1.59 ± 0.04	$(2.39 \pm 0.28) \times 10^{29}$	n	y	n
GRB090516A	4.11	de Ugarte Postigo et al. (2009c)	163.4	1.35 ± 0.02	$(8.42 \pm 1.23) \times 10^{30}$	n	y	y
GRB090519	3.85	Thoene et al. (2009)	58.0	1.23 ± 0.14	$(9.25^{+2.45}_{-2.41}) \times 10^{28}$	n	y	y
GRB090529A	2.63	Malesani et al. (2009a)	70.4	0.70 ± 0.04	$(1.20 \pm 0.31) \times 10^{29}$	n	y	n
GRB090530	1.27	Goldoni et al. (2013)	40.5	0.81 ± 0.02	$(1.13 \pm 0.17) \times 10^{29}$	n	y	y
GRB090618	0.54	Cenko et al. (2009)	113.3	1.15 ± 0.01	$(1.14 \pm 0.05) \times 10^{30}$	n	y	y
GRB090715B	3.00	Wiersema et al. (2009)	266.4	1.20 ± 0.07	$(6.95 \pm 4.05) \times 10^{28}$	n	y	y
GRB090809A	2.74	Malesani et al. (2009b)	8.9	1.20 ± 0.08	$(4.39 \pm 4.24) \times 10^{28}$	y	y	y
GRB090812	2.45	de Ugarte Postigo et al. (2009b)	74.5	1.37 ± 0.10	$(4.37 \pm 0.41) \times 10^{30}$	n	y	y
GRB090814A	0.70	Jakobsson et al. (2009)	78.1	$1.45^{+0.16}_{-0.14}$	$(7.17 \pm 1.83) \times 10^{28}$	y	n	n
GRB090926B	1.24	Fynbo et al. (2009a)	99.3	1.11 ± 0.08	$(3.89 \pm 0.65) \times 10^{29}$	y	n	n
GRB091018	0.97	Chen et al. (2009)	4.4	1.18 ± 0.01	$(7.03 \pm 0.55) \times 10^{29}$	n	y	n
GRB091020	1.71	Xu et al. (2009)	38.9	1.20 ± 0.01	$(2.64 \pm 0.18) \times 10^{30}$	n	y	n
GRB091029	2.75	Chornock et al. (2009b)	39.2	0.81 ± 0.01	$(6.90 \pm 0.66) \times 10^{29}$	n	y	y
GRB091109A	3.08	Rau et al. (2010)	48.0	1.01 ± 0.06	$(4.95 \pm 0.84) \times 10^{29}$	n	n	n
GRB091208B	1.06	Perley et al. (2009b)	14.8	1.06 ± 0.02	$(4.86 \pm 0.66) \times 10^{29}$	n	y	n
GRB100219A	4.67	de Ugarte Postigo et al. (2010)	22.2	1.35 ± 0.05	$(1.06 \pm 0.19) \times 10^{30}$	n	y	n
GRB100302A	4.81	Chornock et al. (2010a)	18.0	0.72 ± 0.03	$(2.68 \pm 0.58) \times 10^{29}$	n	y	y
GRB100316B	1.18	Vergani et al. (2010a)	3.9	1.09 ± 0.06	$(1.17 \pm 0.33) \times 10^{29}$	n	y	n
GRB100316D	0.06	Vergani et al. (2010b)	518.7	1.53 ± 0.01	$(2.31 \pm 1.61) \times 10^{28}$	n	y	n
GRB100418A	0.62	Antonelli et al. (2010)	7.7	0.51 ± 0.03	$(1.89 \pm 0.80) \times 10^{27}$	n	y	y
GRB100424A	2.46	Malesani et al. (2013a)	86.2	2.24 ± 0.16	$(2.49 \pm 0.48) \times 10^{30}$	n	y	n
GRB100425A	1.75	Goldoni et al. (2010)	39.0	0.75 ± 0.03	$(1.17 \pm 0.26) \times 10^{29}$	n	y	y
GRB100513A	4.77	Cenko et al. (2010)	72.5	0.88 ± 0.04	$(1.08 \pm 0.21) \times 10^{30}$	n	y	y
GRB100615A	1.40	Kruehler et al. (2013b)	38.8	0.73 ± 0.02	$(2.04 \pm 0.30) \times 10^{30}$	n	y	n
GRB100621A	0.54	Milvang-Jensen et al. (2010)	63.6	0.97 ± 0.01	$(5.13 \pm 0.49) \times 10^{29}$	n	y	y
GRB100724A	1.29	Thoene et al. (2010)	1.4	1.13 ± 0.05	$(1.23 \pm 0.26) \times 10^{29}$	n	y	n

Continued on next page

GRB	z	z reference	T_{90} (s)	$\alpha_{X,avg,>200s}$	$L_{X,200s}$ (erg cm ⁻² Hz ⁻¹)	Steep Decay Contaminated	Plateau	Flares
GRB100728A	1.57	Kruehler et al. (2013a)	198.6	1.30 ± 0.01	(1.25 ± 0.17) × 10 ³¹	n	y	y
GRB100728B	2.11	Flores et al. (2010)	12.1	1.49 ± 0.07	(1.15 ± 0.22) × 10 ³⁰	n	y	y
GRB100805A	1.85	Oates et al. (2012)	16.7	1.00 ± 0.03	(2.52 ± 0.46) × 10 ²⁹	n	y	y
GRB100814A	1.44	O'Meara et al. (2010)	174.7	1.02 ± 0.01	(1.02 ± 0.09) × 10 ³⁰	n	y	y
GRB100816A	0.80	Tanvir et al. (2010b)	2.6	0.99 ± 0.04	(1.10 ± 0.20) × 10 ²⁹	n	n	y
GRB100901A	1.41	Chornock et al. (2010b)	436.4	1.02 ± 0.02	(1.18 ± 0.25) × 10 ²⁸	y	y	y
GRB100906A	1.73	Tanvir et al. (2010a)	114.6	1.30 ± 0.02	(2.39 ± 0.21) × 10 ³⁰	n	y	y
GRB101219A	0.72	Chornock & Berger (2011)	0.8	2.08 ± 0.22	(1.57 ± 0.42) × 10 ²⁸	n	y	n
GRB101219B	0.55	de Ugarte Postigo et al. (2011b)	44.7	0.64 ± 0.03	(3.49 ± 1.14) × 10 ²⁷	y	y	y
GRB110106B	0.62	Chornock et al. (2011b)	43.5	1.04 ± 0.02	(5.47 ± 0.97) × 10 ²⁸	n	y	y
GRB110128A	2.34	Sparre et al. (2011)	14.2	0.70 ± 0.05	(3.63 ^{+1.02} _{-0.98}) × 10 ²⁸	n	n	n
GRB110205A	2.22	Cenko et al. (2011)	249.4	1.59 ± 0.04	(1.32 ± 0.09) × 10 ³¹	n	n	y
GRB110213A	1.46	Milne & Cenko (2011)	48.0	1.31 ± 0.01	(8.36 ± 1.56) × 10 ²⁹	n	y	n
GRB110422A	1.77	de Ugarte Postigo et al. (2011a)	25.8	1.30 ± 0.01	(8.41 ± 0.56) × 10 ³⁰	n	y	n
GRB110503A	1.61	de Ugarte Postigo et al. (2011c)	10.1	1.17 ± 0.01	(3.52 ± 0.22) × 10 ³⁰	n	y	n
GRB110715A	0.82	Piranomonte et al. (2011)	13.0	1.00 ± 0.01	(1.44 ± 0.14) × 10 ³⁰	n	y	n
GRB110726A	1.04	Cucchiara et al. (2011a)	5.2	1.11 ± 0.11	(5.55 ^{+1.17} _{-1.13}) × 10 ²⁸	n	y	y
GRB110731A	2.83	Tanvir et al. (2011)	40.9	1.21 ± 0.02	(7.10 ± 0.70) × 10 ³⁰	n	y	y
GRB110801A	1.86	Cabrera Lavers et al. (2011)	385.3	1.28 ± 0.04	(3.02 ± 0.32) × 10 ³⁰	n	y	y
GRB110808A	1.35	de Ugarte Postigo et al. (2011d)	40.7	0.72 ± 0.03	(4.53 ± 2.81) × 10 ²⁸	n	y	n
GRB110818A	3.36	D'Avanzo et al. (2011)	102.8	1.19 ± 0.03	(2.07 ± 0.23) × 10 ³⁰	n	y	n
GRB111008A	4.99	Wiersema et al. (2011)	65.3	1.08 ± 0.02	(5.87 ± 0.51) × 10 ³⁰	n	y	n
GRB111107A	2.89	Chornock et al. (2011a)	26.6	0.85 ± 0.05	(5.04 ^{+0.89} _{-0.86}) × 10 ²⁹	n	n	y
GRB111123A	3.15	Xu et al. (2013b)	290.0	1.14 ± 0.03	(1.21 ± 0.23) × 10 ³¹	n	y	y
GRB111209A	0.68	Vreeswijk et al. (2011)	733.4	1.37 ± 0.04	(3.95 ± 0.76) × 10 ³⁰	y	n	y
GRB111215A	2.06	van der Horst et al. (2015)	373.8	1.34 ± 0.01	(1.37 ± 0.14) × 10 ³¹	n	y	y
GRB111225A	0.30	Thoene & de Ugarte Postigo (2014)	105.7	0.94 ± 0.14	(2.52 ± 2.03) × 10 ²⁴	y	y	y
GRB111228A	0.71	Cucchiara & Levan (2011)	101.2	0.90 ± 0.01	(1.20 ± 0.10) × 10 ²⁹	n	y	n
GRB111229A	1.38	Cucchiara et al. (2011b)	439.1	0.59 ± 0.05	(6.88 ± 1.18) × 10 ²⁸	n	y	n
GRB120118B	2.94	Malesani et al. (2013b)	54.7	1.04 ± 0.08	(3.58 ± 2.49) × 10 ²⁹	n	y	y
GRB120119A	1.73	Cucchiara & Prochaska (2012)	68.0	1.40 ± 0.03	(1.67 ± 0.19) × 10 ³⁰	n	y	n
GRB120326A	1.80	Tello et al. (2012)	69.6	0.77 ± 0.03	(5.43 ± 1.11) × 10 ²⁸	n	y	y
GRB120327A	2.81	Kruehler et al. (2012)	63.5	1.25 ± 0.03	(2.18 ^{+0.36} _{-0.33}) × 10 ³⁰	n	y	y
GRB120404A	2.88	Cucchiara & Tanvir (2012)	37.2	1.00 ± 0.05	(1.12 ± 0.14) × 10 ³⁰	n	y	y
GRB120422A	0.28	Schulze et al. (2012)	60.4	0.45 ± 0.03	(2.62 ± 0.95) × 10 ²⁶	n	y	n
GRB120521C	6.00	Tanvir et al. (2012c)	26.7	0.71 ± 0.07	(3.56 ^{+0.91} _{-0.89}) × 10 ²⁹	n	y	n
GRB120712A	4.17	Xu et al. (2012)	14.8	1.31 ± 0.05	(4.67 ± 0.55) × 10 ³⁰	n	n	n
GRB120724A	1.48	Cucchiara et al. (2012)	77.9	0.47 ± 0.09	(1.84 ± 0.61) × 10 ²⁸	n	n	y
GRB120729A	0.80	Tanvir & Ball (2012)	93.9	1.60 ± 0.03	(4.04 ± 0.44) × 10 ²⁹	n	y	n
GRB120802A	3.80	Tanvir et al. (2012a)	50.3	0.62 ± 0.13	(5.55 ± 1.14) × 10 ²⁹	n	y	n
GRB120811C	2.67	Thoene et al. (2012)	26.8	0.98 ± 0.03	(1.64 ± 0.20) × 10 ³⁰	n	y	n
GRB120907A	0.97	Sanchez-Ramirez et al. (2012a)	6.1	0.94 ± 0.02	(1.39 ± 0.15) × 10 ²⁹	n	y	n
GRB120922A	3.10	Knust et al. (2012)	161.4	0.98 ± 0.02	(2.90 ± 0.61) × 10 ³⁰	n	y	y
GRB121024A	2.30	Tanvir et al. (2012d)	68.0	1.17 ± 0.04	(1.76 ± 0.23) × 10 ³⁰	n	y	y
GRB121027A	1.77	Levan et al. (2014)	95.7	0.75 ± 0.02	(4.45 ± 0.75) × 10 ²⁹	n	y	y
GRB121128A	2.20	Tanvir et al. (2012b)	23.4	1.46 ± 0.03	(5.10 ± 0.41) × 10 ³⁰	n	y	y
GRB121201A	3.38	Sanchez-Ramirez et al. (2012b)	38.0	1.15 ± 0.06	(3.43 ± 0.54) × 10 ²⁹	n	n	n
GRB121211A	1.02	Perley et al. (2012)	182.7	0.98 ± 0.03	(5.32 ± 0.74) × 10 ²⁹	n	n	y
GRB121229A	2.71	Fynbo et al. (2012)	86.5	0.69 ± 0.15	(2.71 ± 1.03) × 10 ²⁹	y	n	y
GRB130131B	2.54	Fynbo et al. (2013)	4.3	1.24 ± 0.27	(1.04 ± 0.26) × 10 ³⁰	n	n	y
GRB130408A	3.76	Hjorth et al. (2013)	28.7	1.59 ± 0.06	(7.17 ± 0.74) × 10 ³⁰	n	y	y
GRB130418A	1.22	de Ugarte Postigo et al. (2013a)	274.9	1.47 ± 0.06	(1.25 ± 0.24) × 10 ³⁰	n	y	n
GRB130420A	1.30	de Ugarte Postigo et al. (2013b)	121.1	0.89 ± 0.01	(3.80 ± 0.46) × 10 ²⁹	n	y	n
GRB130427A	0.34	Levan et al. (2013)	241.3	1.28 ± 0.01	(8.16 ± 1.23) × 10 ³⁰	n	y	n
GRB130427B	2.78	Flores et al. (2013)	25.9	1.24 ± 0.05	(7.38 ^{+1.45} _{-1.35}) × 10 ²⁹	n	y	y
GRB130505A	2.27	Tanvir et al. (2013a)	88.5	1.38 ± 0.01	(2.74 ± 0.15) × 10 ³¹	n	y	n
GRB130511A	1.30	Cucchiara & Tanvir (2013)	5.4	1.20 ± 0.05	(1.88 ± 0.32) × 10 ²⁹	n	y	n
GRB130514A	3.60	Schmidl et al. (2013)	191.7	1.02 ± 0.03	(6.48 ± 1.02) × 10 ³⁰	y	n	y
GRB130603B	0.36	Thone et al. (2013)	0.2	1.14 ± 0.03	(2.71 ± 0.34) × 10 ²⁸	n	y	n
GRB130604A	1.06	Cenko et al. (2013)	76.3	0.28 ± 0.29	(5.88 ± 1.50) × 10 ²⁹	n	n	y
GRB130606A	5.91	Castro-Tirado et al. (2013)	262.3	1.35 ± 0.04	(7.27 ± 0.78) × 10 ³⁰	n	n	y
GRB130610A	2.09	Smette et al. (2013)	61.5	1.20 ± 0.04	(7.32 ± 0.96) × 10 ²⁹	n	n	n
GRB130612A	2.01	Tanvir et al. (2013b)	40.5	0.94 ± 0.05	(1.55 ± 0.53) × 10 ²⁹	n	y	y
GRB130701A	1.15	Xu et al. (2013c)	4.4	1.25 ± 0.03	(1.39 ± 0.18) × 10 ³⁰	n	y	n
GRB130831A	0.48	Cucchiara & Perley (2013)	30.2	1.12 ± 0.02	(1.01 ± 0.23) × 10 ²⁹	n	y	y
GRB130907A	1.24	de Ugarte Postigo et al. (2013c)	359.0	1.44 ± 0.12	(3.39 ± 0.19) × 10 ³¹	n	n	y
GRB130925A	0.35	Vreeswijk et al. (2013)	161.1	1.05 ± 0.01	(2.31 ± 0.46) × 10 ³⁰	n	y	y
GRB131004A	0.72	Chornock et al. (2013)	1.5	1.20 ^{+0.21} _{-0.17}	(9.96 ± 2.07) × 10 ²⁸	n	y	y

Continued on next page

GRB	z	z reference	T_{90} (s)	$\alpha_{X,avg,>200s}$	$L_{X,200s}$ (erg cm ⁻² Hz ⁻¹)	Steep Decay Contaminated	Plateau	Flares
GRB131030A	1.29	Xu et al. (2013d)	39.4	1.12 ± 0.01	$(3.99 \pm 0.54) \times 10^{30}$	n	y	y
GRB131103A	0.60	Xu et al. (2013e)	14.7	1.06 ± 0.04	$(7.07 \pm 1.56) \times 10^{28}$	n	y	y
GRB131105A	1.69	Xu et al. (2013a)	111.8	0.84 ± 0.02	$(4.92 \pm 0.67) \times 10^{29}$	n	y	n
GRB131117A	4.04	Hartoog et al. (2013)	10.9	1.03 ± 0.07	$(1.04 \pm 0.19) \times 10^{30}$	n	y	y
GRB131227A	5.30	Cucchiara & Cenko (2013)	18.0	1.36 ± 0.18	$(4.74 \pm 0.98) \times 10^{30}$	n	y	n
GRB140206A	2.73	D'Elia et al. (2014)	93.6	1.05 ± 0.01	$(1.49 \pm 0.08) \times 10^{31}$	n	y	y
GRB140301A	1.42	Kruehler et al. (2014)	36.0	$1.14^{+0.11}_{-0.13}$	$(4.48 \pm 1.08) \times 10^{29}$	n	y	y
GRB140304A	5.30	Jeong et al. (2014)	14.8	2.31 ± 0.12	$(2.07 \pm 0.34) \times 10^{31}$	n	y	y
GRB140318A	1.02	Tanvir et al. (2014)	7.6	0.95 ± 0.08	$(1.30 \pm 0.38) \times 10^{30}$	n	n	n

Table 2 The properties of the GRBs in our sample including our measurements of the correlation parameters and where they are divided in our various sample subsets. Steep decay contamination refers to those light curves where t_{200s} occurs prior to the end of the steep decay phase, so we extrapolate the next segment back to t_{200s} . Plateau/Flares refers to whether or not they are present in the X-ray light curve.

REFERENCES

- Afonso, P., Kruehler, T., Greiner, J., & Klose, S. 2008, GRB Coordinates Network, 8752, 1
- Afonso, P., et al. 2011, A&A, 526, A154
- Amati, L., et al. 2002, A&A, 390, 81
- Antonelli, L. A., et al. 2010, GRB Coordinates Network, 10620, 1
- Bardho, O., Boer, M., & Gendre, B. 2015, ArXiv e-prints
- Barthelmy, S. D., et al. 2005a, Nature, 438, 994
- . 2005b, Space Sci. Rev., 120, 143
- Berger, E. 2009, ApJ, 690, 231
- . 2014, ARA&A, 52, 43
- Berger, E., Foley, R., Simcoe, R., & Irwin, J. 2008a, GRB Coordinates Network, 8434, 1
- Berger, E., & Fox, D. B. 2009, GRB Coordinates Network, 9156, 1
- Berger, E., Fox, D. B., & Cucchiara, A. 2007a, GRB Coordinates Network, 6470, 1
- Berger, E., Fox, D. B., Cucchiara, A., & Cenko, S. B. 2008b, GRB Coordinates Network, 8335, 1
- Berger, E., Kulkarni, S. R., Rau, A., & Fox, D. B. 2006, GRB Coordinates Network, 4815, 1
- Berger, E., & Soderberg, A. M. 2005, GRB Coordinates Network, 4384, 1
- Berger, E., et al. 2005a, ApJ, 634, 501
- . 2005b, ApJ, 629, 328
- . 2007b, ApJ, 664, 1000
- . 2007c, ApJ, 664, 1000
- Boër, M., & Gendre, B. 2000, A&A, 361, L21
- Burrows, D. N., et al. 2005, Space Sci. Rev., 120, 165
- Cabrera Lavers, A., et al. 2011, GRB Coordinates Network, 12234, 1
- Castro-Tirado, A. J., et al. 2013, GRB Coordinates Network, 14796, 1
- Cenko, S. B., Berger, E., Djorgovski, S. G., Mahabal, A. A., & Fox, D. B. 2006, GRB Coordinates Network, 5155, 1
- Cenko, S. B., Gezari, S., Small, T., Fox, D. B., & Chornock, R. 2007, GRB Coordinates Network, 6322, 1
- Cenko, S. B., Hora, J. L., & Bloom, J. S. 2011, GRB Coordinates Network, 11638, 1
- Cenko, S. B., Levan, A. J., & Cucchiara, A. 2013, GRB Coordinates Network, 14762, 1
- Cenko, S. B., et al. 2009, GRB Coordinates Network, 9518, 1
- . 2010, GRB Coordinates Network, 10752, 1
- Chen, H.-W., Helsby, J., Shectman, S., Thompson, I., & Crane, J. 2009, GRB Coordinates Network, 10038, 1
- Chen, H.-W., Prochaska, J. X., Herbert-Fort, S., Christlein, D., & Cortes, S. 2007, GRB Coordinates Network, 6217, 1
- Chincarini, G., et al. 2007, ApJ, 671, 1903
- . 2010, MNRAS, 406, 2113
- Chornock, R., & Berger, E. 2011, GRB Coordinates Network, 11518, 1
- Chornock, R., Berger, E., & Fox, D. 2011a, GRB Coordinates Network, 12537, 1
- Chornock, R., Berger, E., & Fox, D. B. 2011b, GRB Coordinates Network, 11538, 1
- Chornock, R., Cucchiara, A., Fox, D., & Berger, E. 2010a, GRB Coordinates Network, 10466, 1
- Chornock, R., Lunnan, R., & Berger, E. 2013, GRB Coordinates Network, 15307, 1
- Chornock, R., Perley, D. A., Cenko, S. B., & Bloom, J. S. 2009a, GRB Coordinates Network, 9243, 1
- Chornock, R., Perley, D. A., & Cobb, B. E. 2009b, GRB Coordinates Network, 10100, 1
- Chornock, R., et al. 2009c, GRB Coordinates Network, 9151, 1
- . 2010b, GRB Coordinates Network, 11164, 1
- Cucchiara, A., Bloom, J. S., & Cenko, S. B. 2011a, GRB Coordinates Network, 12202, 1
- Cucchiara, A., & Cenko, S. B. 2013, GRB Coordinates Network, 15624, 1
- Cucchiara, A., & Fox, D. B. 2008, GRB Coordinates Network, 7654, 1
- Cucchiara, A., Fox, D. B., & Cenko, S. B. 2007a, GRB Coordinates Network, 7124, 1
- Cucchiara, A., Fox, D. B., Cenko, S. B., & Berger, E. 2008a, GRB Coordinates Network, 8346, 1
- . 2008b, GRB Coordinates Network, 8713, 1
- Cucchiara, A., Fox, D. B., Cenko, S. B., & Price, P. A. 2007b, GRB Coordinates Network, 6083, 1
- Cucchiara, A., & Levan, A. J. 2011, GRB Coordinates Network, 12761, 1
- Cucchiara, A., Levan, A. J., & Tanvir, N. 2011b, GRB Coordinates Network, 12777, 1
- Cucchiara, A., & Perley, D. 2013, GRB Coordinates Network, 15144, 1
- Cucchiara, A., & Prochaska, J. X. 2012, GRB Coordinates Network, 12865, 1
- Cucchiara, A., & Tanvir, N. R. 2012, GRB Coordinates Network, 13217, 1
- . 2013, GRB Coordinates Network, 14621, 1
- Cucchiara, A., Tanvir, N. R., Perley, D., & Levan, A. J. 2012, GRB Coordinates Network, 13512, 1
- Cucchiara, A., et al. 2007c, GRB Coordinates Network, 6665, 1
- . 2011c, ApJ, 736, 7
- Dainotti, M. G., Ostrowski, M., & Willingale, R. 2011, MNRAS, 418, 2202
- Dainotti, M. G., Petrosian, V., Singal, J., & Ostrowski, M. 2013, ApJ, 774, 157
- Dainotti, M. G., Willingale, R., Capozziello, S., Fabrizio Cardone, V., & Ostrowski, M. 2010, ApJ, 722, L215
- D'Avanzo, P., et al. 2011, GRB Coordinates Network, 12284, 1
- . 2012, MNRAS, 425, 506
- De Pasquale, M., Schulze, S., Kann, D. A., Oates, S., & Zhang, B. 2013, in EAS Publications Series, Vol. 61, EAS Publications Series, ed. A. J. Castro-Tirado, J. Gorosabel, & I. H. Park, 217–221
- de Ugarte Postigo, A., Castro-Tirado, A. J., & Gorosabel, J. 2011a, GRB Coordinates Network, 11978, 1
- de Ugarte Postigo, A., Thoene, C. C., Vergani, S. D., Milvang-Jensen, B., & Fynbo, J. 2010, GRB Coordinates Network, 10445, 1
- de Ugarte Postigo, A., et al. 2009a, GRB Coordinates Network, 8766, 1
- . 2009b, GRB Coordinates Network, 9771, 1
- . 2009c, GRB Coordinates Network, 9383, 1

- . 2011b, GRB Coordinates Network, 11579, 1
- . 2011c, GRB Coordinates Network, 11993, 1
- . 2011d, GRB Coordinates Network, 12258, 1
- . 2013a, GRB Coordinates Network, 14380, 1
- . 2013b, GRB Coordinates Network, 14437, 1
- . 2013c, GRB Coordinates Network, 15187, 1
- D’Elia, V., et al. 2008, GRB Coordinates Network, 8531, 1
- . 2014, GRB Coordinates Network, 15802, 1
- Della Valle, M., et al. 2006, *Nature*, 444, 1050
- Dupree, A. K., et al. 2006, GRB Coordinates Network, 4969, 1
- Evans, P. A., et al. 2007, *A&A*, 469, 379
- . 2009, *MNRAS*, 397, 1177
- Falcone, A. D., et al. 2007, *ApJ*, 671, 1921
- Ferrero, P., et al. 2009, *A&A*, 497, 729
- Flores, H., et al. 2010, GRB Coordinates Network, 11317, 1
- . 2013, GRB Coordinates Network, 14493, 1
- Foley, R. J., Chen, H.-W., Bloom, J., & Prochaska, J. X. 2005a, GRB Coordinates Network, 3483, 1
- Foley, R. J., et al. 2005b, GRB Coordinates Network, 4409, 1
- Fong, W., et al. 2013, *ApJ*, 769, 56
- Fugazza, D., et al. 2009, GRB Coordinates Network, 8892, 1
- Fynbo, J. P. U., Malesani, D., Jakobsson, P., & D’Elia, V. 2009a, GRB Coordinates Network, 9947, 1
- Fynbo, J. P. U., et al. 2008, GRB Coordinates Network, 8225, 1
- . 2009b, *ApJS*, 185, 526
- . 2012, GRB Coordinates Network, 14120, 1
- . 2013, GRB Coordinates Network, 14286, 1
- Gao, H., Lei, W.-H., Zou, Y.-C., Wu, X.-F., & Zhang, B. 2013, *New Astronomy Reviews*, 57, 141
- Gehrels, N., et al. 2004, *ApJ*, 611, 1005
- . 2008, *ApJ*, 689, 1161
- Gendre, B., & Boër, M. 2005, *A&A*, 430, 465
- Gendre, B., Galli, A., & Boër, M. 2008, *ApJ*, 683, 620
- Ghirlanda, G., Nava, L., Ghisellini, G., Celotti, A., Burlon, D., Covino, S., & Melandri, A. 2012, *MNRAS*, 420, 483
- Ghirlanda, G., Nava, L., Ghisellini, G., Celotti, A., & Firmani, C. 2009, *A&A*, 496, 585
- Goldoni, P., de Ugarte Postigo, A., & Fynbo, J. P. U. 2013, GRB Coordinates Network, 15571, 1
- Goldoni, P., et al. 2010, GRB Coordinates Network, 10684, 1
- Goldstein, A., et al. 2012, *ApJS*, 199, 19
- Granot, J., & Sari, R. 2002, *ApJ*, 568, 820
- Grupe, D., et al. 2007, *ApJ*, 662, 443
- . 2010, *ApJ*, 711, 1008
- Guetta, D., & Piran, T. 2006, *A&A*, 453, 823
- Hartoog, O. E., et al. 2013, GRB Coordinates Network, 15494, 1
- Hascoët, R., Uhm, Z. L., Mochkovitch, R., & Daigne, F. 2011, *A&A*, 534, A104
- Hjorth, J., Melandri, A., Malesani, D., Kruehler, T., & Xu, D. 2013, GRB Coordinates Network, 14365, 1
- Hjorth, J., et al. 2012, *ApJ*, 756, 187
- Holland, S. 2008, GRB Coordinates Network, 8212, 1
- Jakobsson, P., et al. 2006a, in *American Institute of Physics Conference Series*, Vol. 836, *Gamma-Ray Bursts in the Swift Era*, ed. S. S. Holt, N. Gehrels, & J. A. Nousek, 552–557
- Jakobsson, P., et al. 2006b, GRB Coordinates Network, 5617, 1
- . 2007a, GRB Coordinates Network, 6283, 1
- . 2007b, GRB Coordinates Network, 6398, 1
- . 2009, GRB Coordinates Network, 9797, 1
- Jaunsen, A. O., et al. 2008, *ApJ*, 681, 453
- Jeong, S., Sanchez-Ramirez, R., Gorosabel, J., & Castro-Tirado, A. J. 2014, GRB Coordinates Network, 15936, 1
- Kann, D. A., et al. 2011, *ApJ*, 734, 96
- Kawai, N., et al. 2006, *Nature*, 440, 184
- Knust, F., Kruehler, T., Klose, S., & Greiner, J. 2012, GRB Coordinates Network, 13810, 1
- Kocevski, D., Butler, N., & Bloom, J. S. 2007, *ApJ*, 667, 1024
- Kruehler, T., Fynbo, J. P. U., Milvang-Jensen, B., Tanvir, N., & Jakobsson, P. 2012, GRB Coordinates Network, 13134, 1
- Kruehler, T., Greiner, J., & Kann, D. A. 2013a, GRB Coordinates Network, 14500, 1
- Kruehler, T., Tanvir, N. R., Malesani, D., Xu, D., & Fynbo, J. P. U. 2014, GRB Coordinates Network, 15900, 1
- Kruehler, T., et al. 2013b, GRB Coordinates Network, 14264, 1
- Krühler, T., et al. 2011a, *A&A*, 526, A153
- . 2011b, *A&A*, 534, A108
- . 2012, *ApJ*, 758, 46
- Landsman, W., et al. 2008, GRB Coordinates Network, 8601, 1
- Leibler, C. N., & Berger, E. 2010, *ApJ*, 725, 1202
- Levan, A. J., Cenko, S. B., Perley, D. A., & Tanvir, N. R. 2013, GRB Coordinates Network, 14455, 1
- Levan, A. J., et al. 2014, *ApJ*, 781, 13
- Levesque, E., et al. 2009, GRB Coordinates Network, 9264, 1
- Liang, E., Zhang, B., Virgili, F., & Dai, Z. G. 2007, *ApJ*, 662, 1111
- Liang, E.-W., Racusin, J. L., Zhang, B., Zhang, B.-B., & Burrows, D. N. 2008, *ApJ*, 675, 528
- Liang, E.-W., Yi, S.-X., Zhang, J., Lü, H.-J., Zhang, B.-B., & Zhang, B. 2010, *ApJ*, 725, 2209
- Lien, A., et al. 2015, in-prep
- Malesani, D., et al. 2009a, GRB Coordinates Network, 9457, 1
- . 2009b, GRB Coordinates Network, 9761, 1
- . 2013a, GRB Coordinates Network, 14291, 1
- . 2013b, GRB Coordinates Network, 14225, 1
- Margutti, R., et al. 2010, *MNRAS*, 406, 2149
- . 2013, *MNRAS*, 428, 729
- Melandri, A., et al. 2006, GRB Coordinates Network, 4539, 1
- Milne, P. A., & Cenko, S. B. 2011, GRB Coordinates Network, 11708, 1
- Milvang-Jensen, B., et al. 2010, GRB Coordinates Network, 10876, 1
- Mirabal, N., & Halpern, J. P. 2006, GRB Coordinates Network, 4792, 1
- Mirabal, N., Halpern, J. P., & O’Brien, P. T. 2007, *ApJ*, 661, L127
- Nakar, E., & Piran, T. 2002, *MNRAS*, 330, 920
- Norris, J. P., & Bonnell, J. T. 2006, *ApJ*, 643, 266
- Norris, J. P., Gehrels, N., & Scargle, J. D. 2011, *ApJ*, 735, 23
- Nousek, J. A., et al. 2006, *ApJ*, 642, 389
- Nysewander, M., Fruchter, A. S., & Pe’er, A. 2009, *ApJ*, 701, 824
- Oates, S. R., et al. 2009, *MNRAS*, 395, 490
- . 2012, *MNRAS*, 426, L86
- . 2015, *MNRAS* submitted
- O’Meara, J., Chen, H.-W., & Prochaska, J. X. 2010, GRB Coordinates Network, 11089, 1
- Page, K. L., et al. 2006, *ApJ*, 637, L13
- Panaiteanu, A. 2007, *MNRAS*, 380, 374
- Panaiteanu, A., Mészáros, P., Gehrels, N., Burrows, D., & Nousek, J. 2006, *MNRAS*, 366, 1357
- Perley, D. A., Foley, R. J., Bloom, J. S., & Butler, N. R. 2006, GRB Coordinates Network, 5387, 1
- Perley, D. A., Levan, A. J., Tanvir, N. R., Cenko, S. B., Bloom, J. S., Hjorth, J., Krühler, T., Filippenko, A. V., Fruchter, A., Fynbo, J. P. U., Jakobsson, P., Kalirai, J., Milvang-Jensen, B., Morgan, A. N., Prochaska, J. X., & Silverman, J. M. 2013, *ApJ*, 778, 128
- Perley, D. A., Prochaska, J. X., & Morgan, A. N. 2012, GRB Coordinates Network, 14059, 1
- Perley, D. A., et al. 2008, GRB Coordinates Network, 7889, 1
- . 2009a, *ApJ*, 696, 1871
- . 2009b, GRB Coordinates Network, 10272, 1
- . 2009c, *AJ*, 138, 1690
- Piran, T. 2004, *Reviews of Modern Physics*, 76, 1143
- Piranomonte, S., et al. 2011, GRB Coordinates Network, 12164, 1
- Price, P. A. 2006, GRB Coordinates Network, 5104, 1
- Prochaska, J. X., et al. 2005, GRB Coordinates Network, 3700, 1
- Quimby, R., Fox, D., Hoefflich, P., Roman, B., & Wheeler, J. C. 2005, GRB Coordinates Network, 4221, 1
- Racusin, J. L., et al. 2009, *ApJ*, 698, 43
- . 2011, *ApJ*, 738, 138
- Rau, A., Fynbo, J., & Greiner, J. 2010, GRB Coordinates Network, 10350, 1
- Rau, A., McBreen, S., & Kruehler, T. 2009, GRB Coordinates Network, 9353, 1
- Roming, P. W. A., et al. 2005, *Space Sci. Rev.*, 120, 95
- Rowlinson, A., et al. 2010, *MNRAS*, 408, 383
- Ruiz-Velasco, A. E., et al. 2007, *ApJ*, 669, 1
- Ryan, G., van Eerten, H., MacFadyen, A., & Zhang, B.-B. 2015, *ApJ*, 799, 3
- Sakamoto, T., et al. 2008, *ApJS*, 175, 179
- . 2011, *VizieR Online Data Catalog*, 219, 50002
- Salvaterra, R., et al. 2012, *ApJ*, 749, 68

- Sanchez-Ramirez, R., Gorosabel, J., de Ugarte Postigo, A., & Gonzalez Perez, J. M. 2012a, GRB Coordinates Network, 13723, 1
- Sanchez-Ramirez, R., et al. 2012b, GRB Coordinates Network, 14035, 1
- Sari, R., & Piran, T. 1999, *ApJ*, 520, 641
- Sari, R., Piran, T., & Narayan, R. 1998, *ApJ*, 497, L17
- Sazonov, S. Y., Lutovinov, A. A., & Sunyaev, R. A. 2004, *Nature*, 430, 646
- Schmidl, S., Kann, D. A., & Greiner, J. 2013, GRB Coordinates Network, 14634, 1
- Schulze, S., et al. 2012, GRB Coordinates Network, 13257, 1
- Smette, A., et al. 2013, GRB Coordinates Network, 14848, 1
- Soderberg, A. M., Berger, E., & Ofek, E. 2005, GRB Coordinates Network, 4186, 1
- Soderberg, A. M., et al. 2006, *Nature*, 442, 1014
- . 2007, *ApJ*, 661, 982
- Sparre, M., et al. 2011, GRB Coordinates Network, 11607, 1
- Stanway, E. R., Levan, A. J., Tanvir, N., Wiersema, K., van der Horst, A., Mundell, C. G., & Guidorzi, C. 2015, *MNRAS*, 446, 3911
- Sultana, J., Kazanas, D., & Mastichiadis, A. 2013, *ApJ*, 779, 16
- Tanvir, N., et al. 2009, GRB Coordinates Network, 9219, 1
- Tanvir, N. R., & Ball, J. 2012, GRB Coordinates Network, 13532, 1
- Tanvir, N. R., Fox, D., Fynbo, J., & Trujillo, C. 2012a, GRB Coordinates Network, 13562, 1
- Tanvir, N. R., Kruehler, T., Schulze, S., & Karjalainen, R. 2014, GRB Coordinates Network, 15988, 1
- Tanvir, N. R., Levan, A. J., & Matulonis, T. 2012b, GRB Coordinates Network, 14009, 1
- Tanvir, N. R., Levan, A. J., Matulonis, T., & Smith, A. B. 2013a, GRB Coordinates Network, 14567, 1
- Tanvir, N. R., Wiersema, K., & Levan, A. J. 2010a, GRB Coordinates Network, 11230, 1
- Tanvir, N. R., Wiersema, K., Levan, A. J., Cenko, S. B., & Geballe, T. 2011, GRB Coordinates Network, 12225, 1
- Tanvir, N. R., Wiersema, K., Xu, D., & Fynbo, J. P. U. 2013b, GRB Coordinates Network, 14882, 1
- Tanvir, N. R., et al. 2010b, GRB Coordinates Network, 11123, 1
- . 2012c, GRB Coordinates Network, 13348, 1
- . 2012d, GRB Coordinates Network, 13890, 1
- Tello, J. C., et al. 2012, GRB Coordinates Network, 13118, 1
- Thoenes, C. C., & de Ugarte Postigo, A. 2014, GRB Coordinates Network, 16079, 1
- Thoenes, C. C., et al. 2007a, GRB Coordinates Network, 6379, 1
- . 2007b, GRB Coordinates Network, 6741, 1
- . 2009, GRB Coordinates Network, 9409, 1
- . 2010, GRB Coordinates Network, 10971, 1
- . 2012, GRB Coordinates Network, 13628, 1
- Thone, C. C., de Ugarte Postigo, A., Gorosabel, J., Tanvir, N., & Fynbo, J. P. U. 2013, GRB Coordinates Network, 14744, 1
- Troja, E., King, A. R., O’Brien, P. T., Lyons, N., & Cusumano, G. 2008, *MNRAS*, 385, L10
- van der Horst, A. J., Levan, A. J., Pooley, G. G., Wiersema, K., Krühler, T., Perley, D. A., Starling, R. L. C., Curran, P. A., Tanvir, N. R., Wijers, R. A. M. J., Strom, R. G., Kouveliotou, C., Hartoog, O. E., Xu, D., Fynbo, J. P. U., & Jakobsson, P. 2015, *MNRAS*, 446, 4116
- van Eerten, H., Zhang, W., & MacFadyen, A. 2010, *ApJ*, 722, 235
- van Eerten, H. J., & MacFadyen, A. I. 2011, *ApJ*, 733, L37
- Vergani, S. D., et al. 2010a, GRB Coordinates Network, 10495, 1
- . 2010b, GRB Coordinates Network, 10512, 1
- Vreeswijk, P., Fynbo, J., & Melandri, A. 2011, GRB Coordinates Network, 12648, 1
- Vreeswijk, P. M., Malesani, D., Fynbo, J. P. U., De Cia, A., & Ledoux, C. 2013, GRB Coordinates Network, 15249, 1
- Wiersema, K., Levan, A., Kamble, A., Tanvir, N., & Malesani, D. 2009, GRB Coordinates Network, 9673, 1
- Wiersema, K., et al. 2008, GRB Coordinates Network, 7818, 1
- . 2011, GRB Coordinates Network, 12431, 1
- Xu, D., Fynbo, J. P. U., D’Elia, V., & Tanvir, N. R. 2012, GRB Coordinates Network, 13460, 1
- Xu, D., Malesani, D., Tanvir, N., Kruehler, T., & Fynbo, J. 2013a, GRB Coordinates Network, 15450, 1
- Xu, D., et al. 2009, GRB Coordinates Network, 10053, 1
- . 2013b, GRB Coordinates Network, 14273, 1
- . 2013c, GRB Coordinates Network, 14956, 1
- . 2013d, GRB Coordinates Network, 15407, 1
- . 2013e, GRB Coordinates Network, 15451, 1
- Zhang, B., et al. 2006, *ApJ*, 642, 354
- Zhang, B.-B., Liang, E.-W., & Zhang, B. 2007, *ApJ*, 666, 1002